



ELSEVIER

Physica D 85 (1995) 311–347

PHYSICA D

# Multi-pulse jumping orbits and homoclinic trees in a modal truncation of the damped-forced nonlinear Schrödinger equation

G. Haller<sup>a</sup>, S. Wiggins<sup>b,1</sup>

<sup>a</sup> Division of Applied Mathematics, Brown University, Providence, RI 02912, USA

<sup>b</sup> Department of Applied Mechanics and Department of Control and Dynamical Systems, Caltech 104-44, Pasadena, CA 91125, USA

Received 29 April 1994; revised 6 March 1995; accepted 8 March 1995

Communicated by H. Flaschka

---

## Abstract

In this paper we prove the existence of multi-pulse orbits homoclinic to a slow manifold in a two-mode truncation of the damped-forced nonlinear Schrödinger equation (first suggested by Bishop et al.). These orbits are *jumping*, i.e., the corresponding solutions keep switching in time between neighborhoods of the two characteristic “breathers” of the integrable limit. In the case of no damping, we find multi-pulse Smale horseshoes in the two-mode model, while in the dissipative case we establish the existence of *structurally stable, multi-pulse, heteroclinic connections* between two unstable equilibria. The orbits we construct are not amenable to Melnikov-type perturbation methods. In both the Hamiltonian and the dissipative case we find *homoclinic trees*, which describe the repeated bifurcations of multi-pulse solutions. To illustrate the theoretical predictions, we also present visualizations of these complicated structures.

---

## 1. Introduction

Partial differential equations are often analyzed through finite dimensional reduced models. These models can be studied without the heavy machinery of functional analysis using finite dimensional dynamical systems methods. The reduction of the dimension from infinite to finite can be achieved in several ways, e.g., by applying modal truncations (or Galerkin approximations), Lyapunov–Schmidt reduction, center manifold theory or inertial manifold theory. While the latter three methods have fairly solid mathematical foundations (see, e.g., Marsden and McCracken [27], Mielke [29] and Constantin et al. [5]), they usually involve extensive calculations. Modal truncations are much easier to carry out which makes them very popular in applications (see, e.g., Cascon et al. [4], Holmes [21], Feng and Wiggins [11], etc.). On the other hand, the relation between the modal equations and the full PDE is usually not fully understood.

---

<sup>1</sup> Supported by an NSF Presidential Young Investigator Award, an NSF grant No. DMS-9403691, and an ONR Grant. No. N00014-89-J-3023.

Besides being simple and physically meaningful in most cases, modal truncations can also be extremely useful in another respect: they may admit a particular element in their phase space geometry which is known to be present in the underlying PDE, too. In such cases a thorough understanding of the mode equations can lead to the development of new methods directly applicable to the original infinite dimensional problems. A good example of this situation is the relation between the PDE describing the oscillations of a forced beam and its one-mode truncation, the Duffing oscillator (see Holmes [18] and Holmes and Marsden [19]). Both systems exhibit homoclinic orbits in their unperturbed geometry which give rise to Smale horseshoes in the perturbed problems.

The subject of this paper, a particular two-mode truncation of the damped-driven nonlinear Schrödinger equation (NLS), has also proven itself inspiring for infinite dimensional methods, while being interesting in its own right. It is our hope that our results, which reveal an unexpected level of complexity in this model, again lay the groundwork for a similar direct study of the PDE. Since many finite dimensional problems admit exactly the same structure as the truncated NLS, this paper is also intended as a detailed exposition of the methods we use. Based on what follows, one can directly analyze similar finite dimensional problems (see Section 2 for a list of such problems).

The main topic of this paper originates from the perturbed sine-Gordon equation

$$u_{tt} - u_{xx} + \sin u = \varepsilon(-\hat{\alpha}u_t + \hat{A}u_{txx} + \hat{F}\sin\omega t), \quad (1.1)$$

with boundary conditions

$$u(x = -\frac{1}{2}L, t) = u(x = \frac{1}{2}L, t), \quad u(x, t) = u(-x, t). \quad (1.2)$$

In Eq. (1.1) we let  $0 < \varepsilon\hat{\alpha} \ll 1$ ,  $0 < \varepsilon|\hat{A}| \ll 1$ ,  $\omega = 1 - \varepsilon\tilde{\omega}$ . The constants  $L$  and  $\tilde{\omega}$ , and the perturbation parameter  $\varepsilon$  are all positive. The terms  $\hat{\alpha}u_t$  and  $\hat{A}u_{txx}$  are damping terms. The difference between these two types of damping can be seen through a Fourier modal representation of  $u$ . For  $\hat{\alpha}u_t$  all modes are damped identically and for  $\hat{A}u_{txx}$  the modes with higher wave number are damped more strongly. This can be seen explicitly when we shortly consider a two-mode truncation of the equations.

System (1.1) has been the subject of a series of papers started by the study of Bishop et al. [2,3]. For small amplitudes and frequencies close to 1, one can seek a solution of (1.1) in the form

$$u_\varepsilon(x, t) = 2\sqrt{\varepsilon\tilde{\omega}}[B(X, T)e^{i\omega t} + \bar{B}(X, T)e^{-i\omega t}] + \mathcal{O}(\varepsilon), \quad (1.3)$$

with  $X = \sqrt{2\varepsilon\tilde{\omega}}x$  and  $T = \varepsilon\tilde{\omega}t$ . Substituting (1.3) in (1.1), one arrives at the perturbed nonlinear Schrödinger equation (NLS)

$$-iB_T + B_{XX} + (|B|^2 - 1)B = \varepsilon(i\alpha B - iAB_{XX} + i\bar{F}), \quad (1.4)$$

with  $\hat{\alpha} = 2\varepsilon\tilde{\omega}\alpha$ ,  $\hat{A} = A$ , and  $\hat{F} = 8\varepsilon^{3/2}\tilde{\omega}^{3/2}\bar{F}$ ,  $X \in [-\frac{1}{2}L_X, \frac{1}{2}L_X]$ , and  $L_X = \sqrt{2\varepsilon\tilde{\omega}}L$ . It is well known that for  $\varepsilon = 0$  the NLS is an integrable Hamiltonian system (see Zakharov and Shabat [36]). One can readily verify that this integrable system possesses an invariant plane of solutions with no spatial dependence ( $B_X \equiv 0$ ). Within this plane there is a *circle of fixed points* satisfying  $|B| = 1$ . All points on this circle are interconnected through heteroclinic orbits of the NLS (see Bishop et al. [2], Ablowitz and Herbst [1], and Li and McLaughlin [26]). This “whiskered” circle is in fact a singular limit of a family of whiskered tori which can be studied using the infinite number of conserved quantities of the integrable problem (see Li and McLaughlin [26]). Numerical experiments suggest (Bishop et al. [2]) that the unperturbed homoclinic structure gives rise to characteristic chaotic “jumping” behavior in the perturbed problem: a solitary wave keeps switching in time between two spatially dependent states through a spatially independent state (see Bishop et al. [2] for more

details). Bishop et al. also found that much of this apparent chaotic behavior of system (1.4) is already captured by a two-Fourier-mode truncation

$$B(X, T) = \frac{1}{\sqrt{2}}c(T) + b(T) \cos KX, \quad K = \frac{2\pi}{L_X},$$

which, upon substitution into Eq. (1.4), yields the mode equations

$$\begin{aligned} -i\dot{c} + (|c|^2 + \frac{1}{2}|b|^2 - 1)c + \frac{1}{2}(c\bar{b} + b\bar{c})b &= i\varepsilon(\alpha c + \Gamma), \\ -i\dot{b} + (|c|^2 + \frac{3}{4}|b|^2 - (1 + k^2))b + \frac{1}{2}(c\bar{b} + b\bar{c})c &= i\varepsilon\beta b, \end{aligned} \tag{1.5}$$

with  $\Gamma = \sqrt{2}\bar{\Gamma}$  and  $\beta = \alpha + \Lambda K^2$ . This two-mode model carries several essential features of the underlying PDE (see Kovačič and Wiggins [24] for details):

- it is integrable for  $\varepsilon = 0$ ,
- it is Hamiltonian for  $\alpha = \beta = 0$ ,
- it has an invariant plane given by  $b \equiv 0$ ,
- this plane contains a circle of fixed points satisfying  $|c| = 1$ ,
- the points of this circle are interconnected by heteroclinic orbits which are contained in two symmetric three dimensional manifolds homoclinic to the plane  $b \equiv 0$

These similarities inspired a great deal of work on (1.5) in hope of the better understanding of the chaotic behavior of the NLS. We briefly survey the most important results obtained in previous studies below.

To make use of the  $S^1$  symmetry of the integrable unperturbed model, Kovačič and Wiggins [24] introduced a change of coordinates

$$c = Ie^{-i\phi}, \quad b = (x_1 + ix_2)e^{-i\phi},$$

which puts Eqs. (1.5) in the form

$$\begin{aligned} \dot{x}_1 &= -K^2x_2 - \frac{3}{4}x_1^2x_2 + \frac{1}{4}x_2^3 - \varepsilon \left[ \Gamma \frac{x_2}{\sqrt{2I - x_1^2 - x_2^2}} \sin \phi + \beta x_1 \right], \\ \dot{x}_2 &= (K^2 - 2I)x_1 + \frac{7}{4}x_1^3 + \frac{3}{4}x_1x_2^2 + \varepsilon \left[ \Gamma \frac{x_1}{\sqrt{2I - x_1^2 - x_2^2}} \sin \phi - \beta x_2 \right], \\ \dot{I} &= -\varepsilon \left[ \Gamma \sqrt{2I - x_1^2 - x_2^2} \cos \phi + (\beta - \alpha)(x_1^2 + x_2^2) + 2\alpha I \right], \\ \dot{\phi} &= I - 1 + x_1^2 + \varepsilon \Gamma \frac{1}{\sqrt{2I - x_1^2 - x_2^2}} \sin \phi. \end{aligned} \tag{1.6}$$

They studied system (1.6) under the assumption  $\alpha \neq \beta$  which means unequal damping for different modes ( $\Lambda \neq 0$  in (1.4)). Using geometric singular perturbation theory and a special Melnikov-type method, they showed that for  $\varepsilon > 0$  sufficiently small and

$$\frac{\alpha}{\Gamma} < 0.13, \quad \frac{\beta}{\Gamma} \approx -7.92\sqrt{1 - 2\frac{\alpha^2}{\Gamma}} - 1.14\frac{\alpha}{\Gamma}, \tag{1.7}$$

system (1.6) has a Silnikov-type orbit homoclinic to a saddle-sink-type fixed point. This fixed point lies in an  $\mathcal{O}(\sqrt{\varepsilon})$ -thick resonance band around the resonant circle  $I = 1$  in the invariant plane  $x_1 = x_2 = 0$  of (1.6). Here the term resonance refers to the fact that for  $\varepsilon = 0$  the frequency  $\dot{\phi}$  vanishes on this circle. Although the approach in [24] had fundamental effects on later studies of the model, the Silnikov-type orbits found

in that reference exist only for uneven damping of the modes with  $\alpha > 0$  and  $\beta < 0$ , respectively, which was not the case in the numerical experiments of Bishop et al. In Haller and Wiggins [13] the Hamiltonian limit  $\alpha = \beta = 0$  (no damping) of the two-mode model is analyzed. Using Melnikov's method combined with Fenichel's geometric singular perturbation theory, and some transversality arguments, [13] shows the existence of transverse homoclinic orbits to a family of periodic solutions in the resonance band. This implies the presence of Smale horseshoes and chaotic dynamics on a family of energy surfaces intersecting the resonance band.

Recently, McLaughlin et al. [28] reconsidered the dissipative system (1.6). Extending the techniques used in [24] they established the existence of a symmetric pair of orbits homoclinic to a saddle-saddle-type equilibrium created in the resonance zone. They also showed that when these orbits break, nearby topological horseshoes are created in the dissipative system.

As we mentioned earlier, system (2.1) has also been inspiring for related infinite dimensional studies of the full NLS. Li and McLaughlin [26] (see also Ercolani et al. [6] and Ercolani and McLaughlin [7]) study the unperturbed hyperbolic structure of the NLS in detail. They find that the function space of the integrable limit is foliated by invariant tori. The singular leaves of this foliation contain lower dimensional *whiskered tori*, i.e., tori with homoclinic manifolds.

Another important result is given in Li [25] which is directly motivated by the finite dimensional results in [24] and [28]. Li shows the existence of an orbit homoclinic to a saddle-focus-type equilibrium created in the breakup of the circle of equilibria in the NLS. He also sketches a construction of horseshoes near this orbit which would establish the existence of chaotic dynamics in the infinite dimensional system. As in the similar finite dimensional results of Kovačič and Wiggins [24] and McLaughlin et al. [28], the homoclinic orbit exists on a codimension one set of the parameter space; hence it is not structurally stable.

In this paper, using different methods, we present a new global picture of the homoclinic behavior of the two-mode model both for the undamped and the damped case. The results for the latter case hold on a parameter domain which includes  $\alpha = \beta$  ( $A = 0$ ), the setting of mode independent damping, which was originally studied numerically by Bishop et al. Our main result is the existence of a spatially complicated set of *multi-pulse jumping orbits* which connect various objects created in the resonance band. Here "multi-pulse" means multiple passages near the resonance band followed by fast departures and returns, and "jumping" means alternating passages near the two broken homoclinic manifolds. Such orbits remained hidden to all previous analytical studies described above as *they cannot be detected by Melnikov-type methods*. This is because classical Melnikov methods cannot "track" solutions that make multiple passages near a hyperbolic invariant set.

In the Hamiltonian case, most of the multi-pulse, jumping orbits are transverse homoclinic orbits to "slow" periodic solutions. In the dissipative case they may leave the resonance band in forward or backward time. However, for any element  $N_j \geq 1$  of a certain *pulse sequence*  $\{N_j\}$  of positive integers we are able to prove the existence of *structurally stable, multi-pulse, heteroclinic orbits* which connect two unstable equilibria lying in the dissipative resonance band. The number of such orbits for any  $N_j$  tends to infinity as the perturbation parameter  $\varepsilon$  tends to zero. Most importantly, the bifurcation diagram of multi-pulse orbits is a complicated set which approaches an infinite binary tree as  $\varepsilon, \alpha, \beta \rightarrow 0$ . We are able to compute this *homoclinic tree* explicitly through simple algebraic manipulations. We propose that the spatially and temporally complicated multi-pulse, jumping orbits form an organizing center for the irregular behavior of the two-mode model.

To obtain the above results, we use the *energy-phase method* developed in Haller and Wiggins [15]. For completeness, we present an exposition of this method for the particular case of resonance bands in Section 2 of this paper, with as few technical details as possible. This version of the method is also of independent interest, since it applies to a large class of problems (see Section 2 for a partial list). In our exposition we treat both the purely Hamiltonian and the dissipative case. Accordingly, we study the homoclinic behavior in the forced two-mode model (1.6) with zero dissipation ( $\alpha = \beta = 0$ ) in Section 3.1, then with nonzero dissipation in

Section 3.2. For the former case we present a visualization of the invariant manifolds containing the multi-pulse jumping orbits. We also visualize the *homoclinic tree* mentioned above, and show by explicit calculations how it breaks up under the effect of dissipation. We summarize the results and their implications in Section 4 and speculate about their relationship to the jumping behavior in the underlying PDE.

## 2. Multi-pulse orbits near resonance bands

### 2.1. Set-up

In this section we describe our main tool for the analysis of the truncated NLS. This tool is a special application of a more general global perturbation technique, the *energy-phase method* (see Haller and Wiggins [15]) which is designed to detect multi-pulse homoclinic orbits to slow manifolds of near-integrable two-degree-of-freedom systems (see below for definitions). We will be concerned with systems of the form

$$\begin{aligned} \dot{x} &= JD_x H_0(x, I) + \varepsilon JD_x H_1(x, I, \phi; \varepsilon) + \varepsilon g_x(x, I, \phi, \mu; \varepsilon), \\ \dot{I} &= -\varepsilon D_\phi H_1(x, I, \phi; \varepsilon) + \varepsilon g_I(x, I, \phi, \mu, \varepsilon), \\ \dot{\phi} &= D_I H_0(x, I) + \varepsilon D_I H_1(x, I, \phi, \mu; \varepsilon) + \varepsilon g_\phi(x, I, \phi, \mu; \varepsilon), \end{aligned} \tag{2.1}$$

which is defined on the phase space  $\mathcal{P} = \mathbb{R}^2 \times \mathbb{R} \times S^1$  with the matrix  $J$  given by

$$J = \begin{pmatrix} 0 & 1 \\ -1 & 0 \end{pmatrix}.$$

We will refer to the individual equations in (2.1) as  $(2.1)^x$ ,  $(2.1)^I$  and  $(2.1)^\phi$ , respectively. The above system has a Hamiltonian part deriving from  $H = H_0 + \varepsilon H_1$ , which is assumed to be  $C^{r+1}$  smooth in its arguments with  $r \geq 3$ . The  $C^r$  functions  $g_x$ ,  $g_I$ , and  $g_\phi$  may contain general dissipative terms, and possibly depend on some parameter vector  $\mu \in \mathbb{R}^p$ . Notice that for  $\varepsilon = 0$  (2.1) is integrable with the two integrals  $H_0(x, I)$  and  $I$ . As a result,  $(2.1)_{\varepsilon=0}^x$  decouples from the rest of the equations and can be analyzed as a one-degree-of-freedom Hamiltonian depending on the parameter  $I$ . We make the following assumption on the phase space structure of  $(2.1)^x$ .

**(H1)** There exist  $I_1, I_2 \in \mathbb{R}$ ,  $I_1 < I_2$ , such that for any  $I \in [I_1, I_2]$   $(2.1)_{\varepsilon=0}^x$  has a hyperbolic fixed point,  $\bar{x}^0(I)$ , connected to itself by two homoclinic trajectories,  $x^{h^+}(t, I)$  and  $x^{h^-}(t, I)$ .

Then, considering the Cartesian product of the hyperbolic fixed points with the invariant circles corresponding to the phase variable  $\phi$ , i.e.  $\bar{x}^0(I) \times S^1$  for every  $I \in [I_1, I_2]$ , we obtain an invariant two dimensional manifold  $\mathcal{A}_0$  for system  $(2.1)_{\varepsilon=0}$ . This manifold can conveniently be written in the form

$$\mathcal{A}_0 = \{ (x, I, \phi) \in \mathcal{P} \mid x = \bar{x}^0(I), I \in [I_1, I_2], \phi \in S^1 \}. \tag{2.2}$$

For a more compact formulation of the upcoming results, it will also be useful to think of  $\mathcal{A}_0$  as the image of the annulus  $A = [I_1, I_2] \times S^1$  under the map

$$g_0: (I, \phi) = (\bar{x}^0(I), I, \phi). \tag{2.3}$$

It is easy to see that under assumption (H1),  $\mathcal{A}_0$  has two three dimensional homoclinic manifolds of orbits,  $W_0^+$  and  $W_0^-$ , which contain the two components of its stable and unstable manifolds,  $W^s(\mathcal{A}_0)$  and  $W^u(\mathcal{A}_0)$ ,

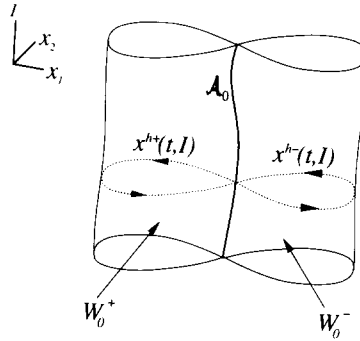


Fig. 1. The manifolds  $\mathcal{A}_0$  and  $W_0$  with the  $\phi$  coordinate suppressed.

respectively (see Fig. 1). The solutions of (2.1) $_{\varepsilon=0}$  on  $W_0^\pm$  can be written in the form

$$y_0^\pm(t, I, \phi_0) = \left( x^{h^\pm}(t, I), I, \phi_0 + \int_0^t D_I H_0(x^{h^\pm}(\tau, I), I) d\tau \right). \tag{2.4}$$

In general the above solutions lie on orbits which are homoclinic to periodic solutions contained in the manifold  $\mathcal{A}_0$ . These periodic solutions satisfy  $I \equiv I_0$ ,  $x \equiv \bar{x}_0(I_0)$ ,  $\dot{\phi} = D_I H(\bar{x}^0(I_0), I_0) \neq 0$ , and their two dimensional stable and unstable manifolds coincide for  $\varepsilon = 0$ . This geometry was studied extensively by several authors, e.g., Holmes and Marsden [20], Robinson [31], and Wiggins [33] in domains of the phase space where the unperturbed frequency  $\dot{\phi} = D_I H_0$  does not vanish restricted to  $\mathcal{A}_0$ . Using generalizations of a method originally due to Melnikov, the above authors gave conditions under which the periodic orbits on  $\mathcal{A}_0$  survive and their stable and unstable manifolds intersect to yield persisting homoclinic orbits in the perturbed problem. Here we will be interested in a case when the above results do not apply. Namely, we will assume that the motion on one of the periodic orbits of  $\mathcal{A}_0$  slows down to zero, giving rise to a circle of fixed points. In precise terms, we will assume the following:

**(H2)** There exists  $I_r \in (I_1, I_2)$  such that

$$D_I H_0(\bar{x}_0(I_r), I_r) = 0,$$

$$m(I_r) = D_I^2 [H_0(\bar{x}_0(I), I)]|_{I=I_r} \neq 0.$$

The notation  $I_r$  refers to the occurrence of a *resonance*: the circle  $C_r$  labelled by  $I = I_r$  in  $\mathcal{A}_0$  can be viewed as a degenerate or *resonant* periodic solution with vanishing frequency  $\dot{\phi}$ . An immediate consequence of this resonance is that the solutions with  $I = I_r$  in  $W_0^\pm$  will connect equilibria lying on the resonant circle  $C_r$ . Two interconnected equilibria will share the same  $x$  and  $I$  coordinates, but their  $\phi$  coordinates will differ by the amount of the net change of  $\phi$  along the connecting heteroclinic orbit. This change,  $\Delta\phi$ , will be referred to as the *phase shift* and using (2.4) it can be written as

$$\Delta\phi^\pm = \int_{-\infty}^{+\infty} D_I H_0(x^{h^\pm}(t, I_r), I) dt, \tag{2.5}$$

where the sign  $\pm$  depends on which of the two homoclinic manifolds we take the connecting orbit from (see Fig. 1). If  $\Delta\phi^\pm$  is an integer multiple of  $2\pi$ , then the points in  $C_r$  are connected to themselves by homoclinic orbits lying in  $W_0^\pm$ . Otherwise, these connections are heteroclinic orbits between different equilibria in  $C_r$ . In either case, the connection orbits form two two-dimensional homoclinic manifolds,  $W_0^+(C_r)$  and  $W_0^-(C_r)$ . This

unperturbed geometry occurs quite frequently in mode interaction problems, such as in Cascon et al. [4], Feng and Sethna [8–10], Feng and Wiggins [11], Nayfeh and Pai [30], Yang and Sethna [35], and Tien and Namamchchivaya [32]. We note that in the general theory in [15]  $D_I H_0$  is allowed to vanish on all of  $\mathcal{A}_0$ , which occurs, e.g., in the systems studied in Holmes [21] and Haller and Wiggins [14].

Our second major assumption on the unperturbed structure of (2.1) is a symmetry hypothesis: we require the two phase shifts  $\Delta\phi^+$  and  $\Delta\phi^-$  to be equal to the same value  $\Delta\phi$ :

**(H3)**

$$\Delta\phi = \int_{-\infty}^{+\infty} D_I H_0(x^{h^+}(t, I_r), I_r) dt \equiv \int_{-\infty}^{+\infty} D_I H_0(x^{h^-}(t, I_r), I_r) dt.$$

For the case of unequal phase shifts the reader is referred to Haller and Wiggins [16].

The invariant manifold  $\mathcal{A}_0$  is normally hyperbolic, which roughly means that stretching rates normal to the manifold dominate the stretching rates in directions tangent to the manifold (see, e.g., Wiggins [34] for precise definitions). As a result of this property, classic theorems guarantee the survival of  $\mathcal{A}_0$  under small perturbations (see, e.g., Fenichel [12] or Wiggins [34]). This means that for  $\varepsilon > 0$  sufficiently small  $\mathcal{A}_0$  perturbs to a  $C^r$   $\varepsilon$ -close invariant manifold  $\mathcal{A}_\varepsilon$  of (2.1) which lies in the image of the annulus  $A$  under a  $C^r$  map

$$g_\varepsilon(I, \phi) = (\bar{x}^\varepsilon(I, \phi), I, \phi) = (\bar{x}^0(I) + \varepsilon x^1(I, \phi, \varepsilon), I, \phi). \tag{2.6}$$

$\mathcal{A}_\varepsilon$  also has surviving stable and unstable manifolds,  $W^s(\mathcal{A}_\varepsilon)$  and  $W^u(\mathcal{A}_\varepsilon)$ , respectively, but they usually split and do not form homoclinic manifolds.

Our main concern will be the following problem: what motions exist on  $\mathcal{A}_\varepsilon$  in a neighborhood of  $I = I_r$  and how are they related to trajectories in  $W^s(\mathcal{A}_\varepsilon)$  and  $W^u(\mathcal{A}_\varepsilon)$ ? To focus on a neighborhood of the resonant action value  $I = I_r$ , we introduce the transformation (see Kovačič and Wiggins [24])

$$I = I_r + \eta\sqrt{\varepsilon}, \quad \eta \in [-\eta_0, \eta_0], \tag{2.7}$$

with  $\eta_0 > 0$  to be determined later. This transformation blows up the *resonance band*

$$\mathcal{P}_{\sqrt{\varepsilon}} = \{(x, I, \phi) \in \mathcal{P} \mid I \in [I_r - \sqrt{\varepsilon}\eta_0, I_r + \sqrt{\varepsilon}\eta_0]\} \tag{2.8}$$

of the phase space  $\mathcal{P}$ . We will be interested to find trajectories of (2.1) for  $\varepsilon > 0$  which are doubly asymptotic to the *near-resonance strip*

$$\mathcal{A}_\varepsilon^R = \mathcal{A}_\varepsilon \cap \mathcal{P}_{\sqrt{\varepsilon}}$$

of the invariant manifold  $\mathcal{A}_\varepsilon$ , which is the image of the annulus

$$\hat{A} = [-\eta_0, \eta_0] \times S^1 \tag{2.9}$$

under the map  $g_\varepsilon \circ b_\varepsilon^{-1}$  with  $b_\varepsilon: A \rightarrow \hat{A}$  defined as

$$b_\varepsilon(I, \phi) = \left( \frac{I - I_r}{\sqrt{\varepsilon}}, \phi \right). \tag{2.10}$$

To describe the homoclinic trajectories of interest more precisely, we introduce the *rotation map*

$$\hat{\mathcal{R}}(\eta, \phi) = (\eta, \phi + \Delta\phi(I_r)), \tag{2.11}$$

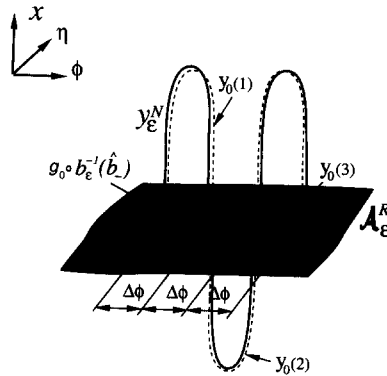


Fig. 2. A 3-pulse orbit homoclinic to  $\mathcal{A}_\epsilon^R$  with jump sequence  $\{+1, -1, +1\}$ .

which rotates objects in the annulus  $\hat{A}$  by the amount of the phase shift  $\Delta\phi$ . We now introduce the following definition.

*Definition 2.1.* Let  $j = \{j_i\}_{i=1}^N$  be a sequence of +1’s and –1’s. We say that an orbit  $y_\epsilon^N$ , homoclinic to the slow manifold  $\mathcal{A}_\epsilon^R$  of system (2.1), is an  $N$ -pulse orbit with jump sequence  $j \equiv j(y_\epsilon^N)$ , if there exists a point  $\hat{b}_- = (0, \phi_-) \in \hat{A}$  and a constant  $\epsilon_0 > 0$ , such that for  $0 < \epsilon < \epsilon_0$  outside a fixed, small neighborhood of  $\mathcal{A}_\epsilon$   $y_\epsilon^N$  is  $C^1$   $\epsilon^{1/4}$ -close to the set

$$Y_j^N = \bigcup_{i=1}^N y_0(i), \tag{2.12}$$

where

$$y_0(i) \subset \begin{cases} W_0^+ & \text{if } j_i = +1, \\ W_0^- & \text{if } j_i = -1, \end{cases} \tag{2.13}$$

is an unperturbed orbit of  $(2.1)_{\epsilon=0}$  asymptotic to the points  $g_0 \circ b_\epsilon^{-1}(\hat{\mathcal{R}}^{i-1}(\hat{b}_-))$  and  $g_0 \circ b_\epsilon^{-1}(\hat{\mathcal{R}}^i(\hat{b}_-))$  in backward and forward time, respectively ( $\hat{\mathcal{R}}^0 \equiv \text{Id}$ ).

For an illustration of this definition see Fig. 2, which shows a 3-pulse orbit with jump sequence +1, –1, +1. Note that, by definition, the  $N$ -pulse orbit is “shadowed” by a sequence of unperturbed heteroclinic orbits which connect points of the resonant circle  $\hat{C}_r$ . The methods we will use give an error of  $\mathcal{O}(\epsilon^{1/4})$  in shadowing multi-pulse orbits and this is exactly the reason for the appearance of an order  $\mathcal{O}(\epsilon^{1/4})$  neighborhood in Definition (2.1). Most of this error occurs when the homoclinic orbit passes by the slow manifold  $\mathcal{A}_\epsilon^R$ , i.e., it leaves a neighborhood of  $y_0(i)$  and starts to follow  $y_0(i + 1)$  (see Haller and Wiggins [15] for details). To find such orbits is fairly easy to do numerically, but to prove their existence is a delicate matter. Melnikov-type arguments do not help in this situation because of the singular nature of the  $\epsilon = 0$  limit of the manifold  $\mathcal{A}_\epsilon^R$ . In the following we will give an analytical criterion which enables one to detect  $N$ -pulse orbits (in the sense of Definition 2.1) in given examples. We will first consider purely Hamiltonian perturbations and then treat the more general dissipative case. For a detailed discussion of the method and for complete proofs the reader is referred to Haller and Wiggins [15].

## 2.2. Hamiltonian perturbations

To apply the energy-phase method in a specific case, one has to perform the following main steps.

1. Identify the dynamics on the slow manifold  $\mathcal{A}_\varepsilon^R$ , at least approximately. This can be done by computing the one-degree-of-freedom *reduced Hamiltonian*  $\hat{\mathcal{H}}(\eta, \phi)$  defined in (2.15) below.
2. For any positive integer  $n$  compute the  $n$ th order energy-difference function  $\Delta^n \hat{\mathcal{H}}(\phi)$  to be defined in (2.18). In a certain sense this function replaces the usual Melnikov-function in the calculation, but it is usually much simpler to evaluate since one does not have to compute improper integrals in the process. In the special case of  $n = 1$  one can show that the energy-difference function coincides with a special Melnikov-function, which was used in Haller and Wiggins [13] to detect single-pulse orbits homoclinic to resonance bands.
3. Based on the zero sets of  $\Delta^n \hat{\mathcal{H}}(\phi)$  associate a pulse number  $N(\hat{\gamma})$  (see (2.23)) to any structurally stable orbit  $\hat{\gamma}$  of the reduced Hamiltonian  $\hat{\mathcal{H}}$ . If this pulse number is well defined, it indicates the existence of a transverse  $N(\hat{\gamma})$ -pulse orbit homoclinic to the slow manifold  $\mathcal{A}_\varepsilon^R$ , which is asymptotic in backward time to a slow orbit approximated by  $\hat{\gamma}$ . For certain parameter values  $N(\hat{\gamma})$  will not be well defined, in which case one can work with the *resonant pulse number*  $N_R(\hat{\gamma})$  (see (2.24)) and obtain the same result without the transversality of the  $N_R(\hat{\gamma})$ -pulse homoclinic orbit.
4. Finally, to describe the shape of the multi-pulse orbits obtained this way, it is enough to determine the jump sequence  $\{j_i\}$  introduced in Definition 2.1. It turns out, that this sequence coincides with the sign sequence  $\chi(\hat{\gamma})$  (see Definition 2.3) which can again be computed based on solely the unperturbed geometry and the reduced Hamiltonian  $\hat{\mathcal{H}}$ .

In the following we will discuss the quantities involved in the above algorithm in detail and formulate the results in precise terms.

### 2.2.1. The dynamics on the manifold $\mathcal{A}_\varepsilon^R$

For purely Hamiltonian perturbations of system (2.1) <sub>$\varepsilon=0$</sub>  we have  $g \equiv 0$ . In this case the solutions of the perturbed system are still confined to energy level surfaces of the form

$$E_\varepsilon(h) = \{ (x, I, \phi) \in \mathcal{P} \mid H(x, I, \phi; \varepsilon) = h \}. \quad (2.14)$$

Using a Taylor expansion in  $\varepsilon$  one can see that for small  $\varepsilon > 0$  the solutions on the manifold  $\mathcal{A}_\varepsilon^R$  will be close to the level curves of the *reduced Hamiltonian*

$$\hat{\mathcal{H}}(\eta, \phi) = \frac{1}{2}m(I_r)\eta^2 + H_1(\bar{x}^0(I_r), I_r, \phi; 0), \quad (2.15)$$

with  $m(I_r)$  defined in hypothesis (H2). More precisely, in  $\mathcal{A}_\varepsilon^R$  the dynamics is governed by a one-degree-of-freedom *reduced system* of the form

$$\begin{pmatrix} \dot{\phi} \\ \dot{\eta} \end{pmatrix} = \sqrt{\varepsilon} JD_{(\phi, \eta)} \hat{\mathcal{H}} + \mathcal{O}(\sqrt{\varepsilon^2}). \quad (2.16)$$

The characteristic time scale of this system is  $\mathcal{O}(\sqrt{\varepsilon})$ , which shows that  $\mathcal{A}_\varepsilon^R$  is a “*slow manifold*”.

Formally, the reduced Hamiltonian  $\hat{\mathcal{H}}$  is defined on the annulus  $\hat{A}$ , but we can use the projection map

$$\Pi_\varepsilon = b_\varepsilon \circ g_\varepsilon^{-1}: \mathcal{A}_\varepsilon^R \rightarrow \hat{A} \quad (2.17)$$

to project orbits from the slow manifold  $\mathcal{A}_\varepsilon^R$  to the annulus  $\hat{A}$  and compare them to the level curves of  $\hat{\mathcal{H}}$ . (2.16) shows that for any structurally stable orbit of  $\hat{\mathcal{H}}$ ,  $\hat{\gamma}_0 \subset \hat{A}$ , we can find a slow orbit  $\gamma_\varepsilon \subset \mathcal{A}_\varepsilon^R$  of (2.1) such that  $\hat{\gamma}_0$  and the projection  $\Pi_\varepsilon(\gamma_\varepsilon)$  are  $C^{r-2} \sqrt{\varepsilon}$ -close in  $\hat{A}$ .

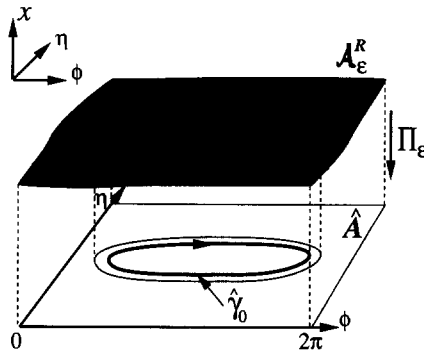


Fig. 3. The relation between slow orbits on  $\mathcal{A}_\varepsilon^R$  and internal orbits of  $\hat{\mathcal{H}}$ .

**Definition 2.2.** We will call a non-equilibrium orbit of  $\hat{\mathcal{H}}$  an *internal orbit*, if it is structurally stable under Hamiltonian perturbations and it is isolated from the boundary of  $\hat{A}$ .

In view of our discussion above, all internal orbits of  $\hat{\mathcal{H}}$  indicate orbits on the slow manifold  $\mathcal{A}_\varepsilon^R$  whose projection on  $\hat{A}$  are  $\mathcal{O}(\sqrt{\varepsilon})$  close to the corresponding internal orbits (see Fig. 3). The sets of orbits forward (backward) asymptotic to an orbit  $\gamma_\varepsilon \subset \mathcal{A}_\varepsilon$  will be denoted by  $W^s(\gamma_\varepsilon)$  ( $W^u(\gamma_\varepsilon)$ ). The multi-pulse orbits (see Definition 2.1) we will construct in this subsection will lie in the intersection of stable and unstable manifolds of slow orbits on  $\mathcal{A}_\varepsilon^R$ .

2.2.2. *Energy-difference functions*

For any positive integer  $n$  we define the  $n$ th order energy-difference function,  $\Delta^n \hat{\mathcal{H}}$ , as

$$\begin{aligned} \Delta^n \hat{\mathcal{H}}(\phi) &= \hat{\mathcal{H}}(\eta, \phi + n\Delta\phi) - \hat{\mathcal{H}}(\eta, \phi) \\ &= H_1(\bar{x}^0(I_r), I_r, \phi + n\Delta\phi; 0) - H_1(\bar{x}^0(I_r), I_r, \phi; 0), \end{aligned} \tag{2.18}$$

and its zero set

$$\hat{V}_-^n = \{ (\eta, \phi) \in \hat{A} \mid \Delta^n \hat{\mathcal{H}}(\phi) = 0 \}. \tag{2.19}$$

Note that  $\Delta^n \hat{\mathcal{H}}$  contains *energy*-type information from the perturbed problem and *phase*-type information from the unperturbed problem. Also note that it roughly measures the leading order energy difference between points of  $\mathcal{A}_\varepsilon^R$  which were formerly connected by heteroclinic orbits.

We will particularly be interested in the transverse zeros of  $\Delta^n \hat{\mathcal{H}}$ , which are contained in the set

$$\hat{Z}_-^n = \{ (\eta, \phi) \in V_-^n \mid D_\phi \Delta^n \hat{\mathcal{H}}(\phi) \neq 0 \}. \tag{2.20}$$

We will also need the  $n\Delta\phi$  translates of these sets in the  $\phi$  coordinate direction, so we define

$$\hat{V}_+^n = \hat{\mathcal{R}}^n(\hat{V}_-^n), \quad \hat{Z}_+^n = \hat{\mathcal{R}}^n(\hat{Z}_-^n), \tag{2.21}$$

where the map  $\hat{\mathcal{R}}$  is defined in analogy with the rotation map  $\mathcal{R}$ , but on the annulus  $\hat{A}$ , i.e.,

$$\begin{aligned} \hat{\mathcal{R}}: \hat{A} &\rightarrow \hat{A}, \\ (\eta, \phi) &\mapsto (\eta, \phi + \Delta\phi). \end{aligned}$$

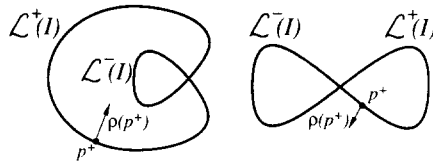


Fig. 4. The definition of the normal  $\rho(p^+)$  in two possible cases.

Finally, for later notational convenience (see (2.23) and (2.24) below), we introduce the definition

$$\hat{V}_-^0 = \emptyset. \tag{2.22}$$

### 2.2.3. Pulse numbers

To describe multi-pulse connections between orbits in  $\mathcal{A}_e^R$ , we will associate pulse numbers to the  $\alpha$ -limit sets of these connections. To this end, for any internal orbit  $\hat{\gamma} \subset \hat{A}$  of  $\hat{\mathcal{H}}$  we define the *pulse number*

$$N(\hat{\gamma}) = \min\{ n \geq 1 \mid \hat{V}_-^k \cap \hat{\gamma} = \emptyset, k = 0, \dots, n - 1, \hat{Z}_-^n \cap \hat{\gamma} \neq \emptyset \}, \tag{2.23}$$

where the symbol  $\cap$  refers to *nonempty transversal intersection*. In words, the pulse number of a given internal orbit  $\hat{\gamma}$  of  $\hat{\mathcal{H}}$  is the minimum index  $n$  such that the intersection of  $\hat{\gamma}$  with  $V_-^k$  is empty for  $k = 0, \dots, n - 1$ , but  $\hat{\gamma}$  has a nonempty transversal intersection with  $Z_-^n$ . (A little bit of thinking shows that the geometric meaning of  $N(\hat{\gamma})$  is the following: it equals the minimum number of rotations of  $\hat{\gamma}$  by the amount of the phase shift  $\Delta\phi$  in the annulus  $\hat{A}$ , such that the rotated image of  $\hat{\gamma}$  intersects transversally an internal orbit of  $\hat{\mathcal{H}}$  with the same energy).

A frequent situation when  $N(\gamma)$  may not be defined is when the phase shift  $\Delta\phi$  is constant and “resonates” with  $2\pi$ , i.e., there exist relative prime positive integers  $N$  and  $k$  such that  $N\Delta\phi(I) \equiv 2k\pi$ . In this case the zero set  $V_-^N$  equals the whole annulus  $\hat{A}$  itself, and  $Z_-^N = \emptyset$ . As a result, if  $\hat{\gamma}$  does not intersect  $V_-^k$  for  $k = 1, \dots, N - 1$  then the pulse number  $N(\hat{\gamma})$  is not defined. To treat such a situation we introduce the resonant pulse number

$$N_R(\hat{\gamma}) = \min\{ n \geq 1 \mid \hat{V}_-^k \cap \hat{\gamma} = \emptyset, k = 0, \dots, n - 1, \hat{V}^n \equiv \hat{A} \}. \tag{2.24}$$

### 2.2.4. Sign sequences

Before formulating an existence result on multi-pulse orbits homoclinic to  $\mathcal{A}_e^R$ , we need one more technical ingredient. Let us consider the homoclinic loops

$$\mathcal{L}^+(I) = \{x^{h^+}(t; I)\}_{t=-\infty}^{+\infty}, \quad \mathcal{L}^-(I) = \{x^{h^-}(t; I)\}_{t=-\infty}^{+\infty}. \tag{2.25}$$

The loop  $\mathcal{L}^+(I)$  divides the  $(x_1, x_2)$  plane into two disjoint open sets, the exterior of  $\mathcal{L}^+(I)$ , denoted  $\text{Ext}(\mathcal{L}^+(I))$ , and the interior of  $\mathcal{L}^+(I)$ , denoted  $\text{Int}(\mathcal{L}^+(I))$ . Let us pick a point  $p^+ \in \mathcal{L}^+(I)$  and let  $\rho(p^+)$  denote the unit normal to  $\mathcal{L}^+(I)$  at the point  $p^+$  pointing in the direction of the other homoclinic loop  $\mathcal{L}^-(I)$ . In other words,  $\rho(p^+)$  points to  $\text{Ext}(\mathcal{L}^+(I))$  if  $\mathcal{L}^-(I) \subset \text{Ext}(\mathcal{L}^+(I))$ , and  $\rho(p^+)$  points to  $\text{Int}(\mathcal{L}^+(I))$  if  $\mathcal{L}^-(I) \subset \text{Int}(\mathcal{L}^+(I))$ , as shown in Fig. 4. We define the sign constant

$$\sigma = \text{sign} \langle D_x H_0|_{p^+}, \rho(p^+) \rangle. \tag{2.26}$$

Note that  $\sigma$  is independent of  $I$  and of the choice of  $p^+$  by the normal hyperbolicity of the unperturbed manifold  $\mathcal{A}_0$ .  $\sigma$  also remains the same if we interchange the roles of  $\mathcal{L}^+(I)$  and  $\mathcal{L}^-(I)$ . Using the sign constant  $\sigma$  we now associate sign sequences to internal orbits of the reduced Hamiltonian  $\mathcal{H}$ .

**Definition 2.3.** Let  $\hat{\gamma}$  be an internal orbit of the reduced Hamiltonian  $\hat{\mathcal{H}}$  and suppose that  $N(\hat{\gamma}) = N$ . Then the positive sign sequence  $\chi^+(\hat{\gamma}) = \{\chi_k^+(\hat{\gamma})\}_{k=1}^N$  of  $\hat{\gamma}$  is defined as

$$\chi_1^+(\hat{\gamma}) = +1, \quad \chi_{k+1}^+(\hat{\gamma}) = \sigma \operatorname{sign}(\Delta^k \hat{\mathcal{H}}|_{\hat{\gamma}}) \chi_k^+(\hat{\gamma}), \quad k = 1, \dots, N - 1. \tag{2.27}$$

The negative sign sequence of  $\hat{\gamma}$  is defined as  $\chi^-(\hat{\gamma}) = -\chi^+(\hat{\gamma})$ .

Note that the assumption  $N(\gamma) = N$  is important for the sign sequences to be well defined, since generally  $\hat{\mathcal{H}}$  takes different values on points of  $\hat{\mathcal{R}}^k(\hat{\gamma})$ . However, it follows from the definition of  $N$  that none of these values is equal to  $\hat{\mathcal{H}}|_{\hat{\gamma}}$  for  $k = 1, \dots, N - 1$  otherwise  $\hat{\gamma}$  would intersect the zero set  $\hat{V}^k$  contradicting the fact that  $N(\hat{\gamma}) = N$ . Consequently, by the continuity of  $\hat{\mathcal{H}}$  on  $\hat{\mathcal{R}}^k(\hat{\gamma})$ , either  $\hat{\mathcal{H}}|_{\hat{\mathcal{R}}^k(\hat{\gamma})} > \hat{\mathcal{H}}|_{\hat{\gamma}}$  or  $\hat{\mathcal{H}}|_{\hat{\mathcal{R}}^k(\hat{\gamma})} < \hat{\mathcal{H}}|_{\hat{\gamma}}$  holds, and  $\chi_{k+1}^+$  is well defined.

**2.2.5. The existence of  $N$ -pulse orbits homoclinic to  $\mathcal{A}_\varepsilon^R$**

Our main result in this subsection will be the following: Suppose that for an internal orbit  $\hat{\gamma}_0^-$  of the reduced Hamiltonian  $N(\hat{\gamma}_0^-) = N$ . Then there is a slow orbit  $\gamma_\varepsilon^-$  on  $\mathcal{A}_\varepsilon^R$ , with  $\Pi_\varepsilon(\gamma_\varepsilon^-) \mathcal{O}(\sqrt{\varepsilon})$ -close to  $\hat{\gamma}_0^-$ , such that  $\gamma_\varepsilon^-$  is the backward limit set of two  $N$ -pulse transverse homoclinic orbits to  $\mathcal{A}_\varepsilon^R$ . Furthermore, the jump sequences of these  $N$ -pulse orbits are given exactly by the sign sequences  $\chi^+(\hat{\gamma}_0^-)$  and  $\chi^-(\hat{\gamma}_0^-)$ . The homoclinic orbits leave a neighborhood of  $\mathcal{A}_\varepsilon^R$  near the point  $\Pi_\varepsilon^{-1}(\hat{b}_-)$  and finally return to  $\mathcal{A}_\varepsilon^R$  near the point  $\Pi_\varepsilon^{-1}(\hat{b}_+)$ , where  $g_0$  is defined in (2.3) and

$$\hat{b}_- = \hat{\gamma}_0^- \cap \hat{Z}_-^N, \quad \hat{b}_+ = \hat{\mathcal{R}}^N(\hat{b}_-). \tag{2.28}$$

Furthermore, the positive limit set,  $\gamma_\varepsilon^+$ , of the homoclinic orbits projects down under  $\Pi_\varepsilon$  close to an internal orbit  $\hat{\gamma}_0^+$  of  $\hat{\mathcal{H}}$  which passes through  $\hat{b}_+$ . Hence, for, say,  $N = 3$  one may obtain the existence of an orbit shown in Fig. 2 based on the knowledge of the reduced Hamiltonian  $\hat{\mathcal{H}}$  and the location of the zero sets of the energy-difference function  $\Delta^N \hat{\mathcal{H}}$ . The following theorem formulates all this in more precise terms.

**Theorem 2.1.** Assume that hypotheses (H1)–(H3) hold and  $g \equiv 0$  in system (2.1). Suppose that for an internal orbit  $\hat{\gamma}_0^- \subset \hat{A}$  of the reduced Hamiltonian  $\hat{\mathcal{H}}$

(A1)  $N \equiv N(\hat{\gamma}_0^-)$  is defined,

(A2) Let  $\hat{b}_-$  and  $\hat{b}_+$  defined as in (2.28). Assume that the orbit  $\hat{\gamma}_0^+ \subset \hat{A}$  of the reduced Hamiltonian  $\hat{\mathcal{H}}$  which contains  $\hat{b}_+$  is an internal orbit with  $\hat{Z}_+^N \cap \hat{\gamma}_0^+$  (see Fig. 5).

Then there exists  $\varepsilon_0 > 0$  such that for  $0 < \varepsilon < \varepsilon_0$

(i) The slow manifold  $\mathcal{A}_\varepsilon^R$  has two  $N$ -pulse homoclinic orbits,  $y_\varepsilon^{N+}$  and  $y_\varepsilon^{N-}$  with jump sequences  $\chi^+(\hat{\gamma}_0^-)$  and  $\chi^-(\hat{\gamma}_0^-)$ , respectively, which are positively asymptotic to an internal orbit  $\gamma_\varepsilon^+ \subset \mathcal{A}_\varepsilon^R$  and negatively

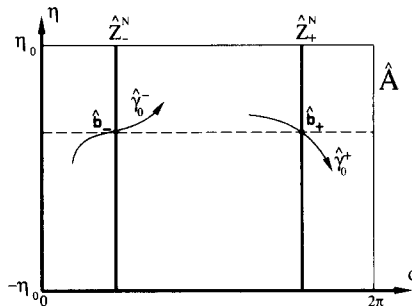


Fig. 5. Assumption (A2) of Theorem 2.1.

asymptotic to an internal orbit  $\gamma_\epsilon^- \subset \mathcal{A}_\epsilon^R$ . Moreover, the projections  $\Pi_\epsilon(\gamma_\epsilon^-)$  and  $\Pi_\epsilon(\gamma_\epsilon^+)$  are  $\mathcal{O}(\sqrt{\epsilon})$ -close to  $\hat{\gamma}_0^-$  and  $\hat{\gamma}_0^+$ , respectively.

(ii)  $y_\epsilon^{N+}$  and  $y_\epsilon^{N-}$  lie in the intersection of  $W^u(\gamma_\epsilon^-)$  and  $W^s(\gamma_\epsilon^+)$ , which is transversal within the energy surface  $E_\epsilon(h)$  with  $h = H|_{\gamma_\epsilon^+} = H|_{\gamma_\epsilon^-}$ .

(iii) Suppose that  $\hat{\gamma}_0^- \equiv \hat{\gamma}_0^+$ . Then  $\gamma_\epsilon^- \equiv \gamma_\epsilon^+$ . In particular, if  $\hat{\gamma}_0^-$  is a periodic orbit, then  $\hat{\gamma}_\epsilon^-$  is a periodic orbit which has at least two transverse homoclinic orbits. As a result, system (2.1) has Smale horseshoes on energy surfaces near  $H = H|_{\gamma_\epsilon^-}$ .

Suppose now that instead of assumption (A1) above we have

(A1')  $N \equiv N_R(\hat{\gamma}_0^-)$  is defined.

Then statements (i)–(iii) still hold with the exception of the transversality of the  $N$ -pulse orbits and the existence of Smale horseshoes.

*Proof.* The main idea of the proof is to follow the unstable manifolds of slow orbits as they leave an  $\mathcal{O}(\epsilon^{1/4})$  neighborhood,  $U$ , of the slow manifold  $\mathcal{A}_\epsilon^R$  and then later return to it. As in the usual construction of orbits homoclinic to equilibria (see, e.g., Wiggins [33]), one can define a global and a local map to track the above-mentioned departures and returns repeatedly. It turns out that the projections of these maps on the annulus  $\hat{A}$  are well defined. Moreover, the projected local map is  $C^1$ -close to the identity map provided the unstable manifold of a given slow orbit does not intersect the local stable manifold of that orbit upon reentering  $U$ . Furthermore, the projected global map is  $C^1$ -close to a shift in  $\hat{A}$  by the amount of the phase shift, which is given by the rotation map  $\hat{\mathcal{R}}$  defined in (2.11). Hence,  $N$  excursions of the unstable manifold  $W^u(\gamma_\epsilon^-)$  of a slow orbit  $\gamma_\epsilon$  can be approximated by applying  $\hat{\mathcal{R}}^N$  to the projection of  $W^u(\gamma_\epsilon)$  on  $\hat{A}$ . However, this projection will be close to a level curve  $\hat{\gamma}_0^-$  of the reduced Hamiltonian  $\hat{\mathcal{H}}$ , so one can apply  $\hat{\mathcal{R}}^N$  to  $\hat{\gamma}_0^-$ . One can show that if  $\hat{\mathcal{R}}^N(\hat{\gamma}_0^-)$  intersects another level curve,  $\hat{\gamma}_0^+$ , of  $\hat{\mathcal{H}}$  with  $\hat{\mathcal{H}}|\hat{\gamma}_0^- = \hat{\mathcal{H}}|\hat{\gamma}_0^+$ , then there exists a slow orbit  $\gamma_\epsilon^-$  such that  $W^u(\gamma_\epsilon^-)$  intersects  $W_{loc}^s(\gamma_\epsilon^+)$  upon its  $n$ th return to the tubular neighborhood  $U$ . Hence, to obtain an  $n$ -pulse orbit connecting slow orbits on  $\mathcal{A}_\epsilon^R$ , one needs to look for transverse zeros of the expression  $\hat{\mathcal{H}}(\eta, \phi + n\Delta\phi) - \hat{\mathcal{H}}(\eta, \phi)$ , which is just the  $n$ th order energy-difference function defined in (2.18). One has to find the minimal index  $n$  for each reduced orbit  $\hat{\gamma}_0^-$  such that  $\hat{\gamma}_0^-$  contains a zero of  $\Delta^n \hat{\mathcal{H}}$ , otherwise the approximation for the local map described above breaks down. This naturally leads to the definition of the pulse number  $N(\hat{\gamma}_0^-)$  introduced in (2.23). Identifying the shape of the multi-pulse orbits constructed this way means finding the jump sequence appearing in Definition 2.1. This essentially means verifying on which side of the hypersurface  $W_{loc}^s(\mathcal{A}_\epsilon)$  the multi-pulse orbit ends up after its  $k$ th pulse. Knowing the direction of the gradient of  $H$ , this can be checked by comparing the energy of  $W^u(\gamma_\epsilon^-)$  to the energies of nearby orbits in  $W_{loc}^s(\mathcal{A}_\epsilon)$ . One finds that this is the same as comparing the energy  $\hat{\mathcal{H}}|\hat{\gamma}_0^-$  to the energies of the level curves of  $\hat{\mathcal{H}}$  which intersect  $\hat{\mathcal{R}}^k(\hat{\gamma}_0^-)$ . This directly leads to the expressions for the sign sequences appearing in Definition 2.3, which therefore are equal to the jump sequences of two multi-pulse orbits. For details of the arguments we sketched here the reader is referred to Haller and Wiggins [15].  $\square$

To apply the above theorem one has to compute the pulse number  $N(\hat{\gamma})$  or  $N_R(\hat{\gamma})$  for all internal orbits  $\hat{\gamma}$  of interest (see assumption (A1)). This computation depends on the particular problem, but for internal orbits near local minima or maxima of the reduced Hamiltonian  $\hat{\mathcal{H}}$  one can universally follow the procedure we will use in Section 3.1.2 (see Haller and Wiggins [15] for another example where the same computation works).

### 2.3. Dissipative perturbations

We now turn to the more general case of nonzero dissipation in system (2.1), i.e., we drop the requirement  $g \equiv 0$ . The simplest way to extend the results of the Hamiltonian limit to this case is to assume that the dissipative perturbation is much smaller than the Hamiltonian perturbation. Under this assumption one can show that the multi-pulse orbits homoclinic to  $\mathcal{A}_\varepsilon^R$  obtained for Hamiltonian perturbations survive but their asymptotics changes according to the weakly dissipative dynamics on  $\mathcal{A}_\varepsilon^R$ . Here we will not deal with such weakly dissipative perturbations; instead we will allow the dissipation to be of the same order as the Hamiltonian perturbation terms deriving from  $H_1$ .

#### 2.3.1. The dynamics on the manifold $\mathcal{A}_\varepsilon^R$

As one again finds from a simple Taylor expansion, the dynamics on the persisting slow manifold  $\mathcal{A}_\varepsilon^R$  can be approximated by the *dissipative reduced system*

$$\begin{aligned} \dot{\eta} &= -D_\phi \hat{\mathcal{H}}_D(\eta, \phi) + \sqrt{\varepsilon} D_I g_I(\bar{x}^0(I_r), I_r, \phi; 0) \eta, \\ \dot{\phi} &= D_\eta \hat{\mathcal{H}}_D(\eta, \phi) + \sqrt{\varepsilon} g_\phi(\bar{x}^0(I_r), I_r, \phi; 0), \end{aligned} \tag{2.29}$$

where the function  $\hat{\mathcal{H}}_D$  is of the form

$$\hat{\mathcal{H}}_D(\eta, \phi) = \hat{\mathcal{H}}(\eta, \phi) - \int_0^\phi g_I(\bar{x}^0(I_r), I_r, u; 0) du, \tag{2.30}$$

with  $\hat{\mathcal{H}}$  being the same as in (2.15). For  $\varepsilon = 0$  (2.29) is a locally Hamiltonian system. Locality comes from the fact that  $\hat{\mathcal{H}}_D$  is not necessarily periodic in  $\phi$ , so it does not necessarily give a single valued Hamiltonian on the annulus  $\hat{A}$ . However, on fixed regions  $[-\eta_0, \eta_0] \times [\phi_0, \phi_1]$ ,  $\phi_1 - \phi_0 < 2\pi$ ,  $\hat{\mathcal{H}}_D$  is a Hamiltonian for  $(2.29)_{\varepsilon=0}$ .

*Definition 2.4.* We will call a non-equilibrium orbit  $\hat{\gamma} \subset \hat{A}$  of the reduced system  $(2.29)_{\varepsilon=0}$  an *internal orbit*, if it is structurally stable with respect to locally Hamiltonian perturbations.

We want the system (2.29) to be truly dissipative for  $\varepsilon > 0$ , which can be guaranteed by the nondegeneracy condition

**(H4)**

$$D_I g_I(\bar{x}^0(I_r), I_r, \phi; 0) + D_\phi g_\phi(\bar{x}^0(I_r), I_r, \phi; 0) \neq 0.$$

Under this assumption the reduced system (2.29) approximates compact segments of the orbits on the slow manifold  $\mathcal{A}_\varepsilon^R$  with an  $\mathcal{O}(\varepsilon)$  precision. Note however, that for  $\varepsilon > 0$  there may be no orbits of (2.29), other than fixed points, which are isolated from  $\partial \hat{A}$ . This is related to the fact that for non-Hamiltonian perturbations  $\mathcal{A}_\varepsilon^R$  is usually an overflowing or inflowing invariant manifold, i.e., it is invariant only in one time direction.

For what follows we assume that

**(H5)** For any two unperturbed solutions  $y_0^+(t, I_r, \phi_0^+)$  and  $y_0^-(t, I_r, \phi_0^-)$  of  $(2.1)_{\varepsilon=0}$  with  $y_0^+(t, I_r, \phi_0^+) \in W_0^+$  and  $y_0^-(t, I_r, \phi_0^-) \in W_0^-$  for all  $t \in \mathbb{R}$  and with

$$\lim_{t \rightarrow -\infty} y_0^+(t, I_r, \phi_0^+) = \lim_{t \rightarrow -\infty} y_0^-(t, I_r, \phi_0^-),$$

the following is satisfied:

$$\int_{-\infty}^{+\infty} \langle DH_0, g \rangle|_{y_0^+(t, I_r, \phi_0^+)} dt = \int_{-\infty}^{+\infty} \langle DH_0, g \rangle|_{y_0^-(t, I_r, \phi_0^-)} dt.$$

This assumption simplifies the formulation of the upcoming results and it holds for all applications we know of, including the two-mode truncation of the damped, driven NLS equation studied in this paper. (H5) implies that the improper integrals in (2.31) below do not depend on which of the two unperturbed homoclinic manifolds the particular solution  $y^i(t)$  belongs to.

### 2.3.2. Energy-difference functions

In the dissipative case we define the  $n$ th order energy-difference function in the following way:

$$\Delta^n \hat{\mathcal{H}}_D(\phi) = \Delta^n \hat{\mathcal{H}}(\phi) - \sum_{i=1}^n \int_{-\infty}^{+\infty} \langle DH_0, g \rangle|_{y^i(t)} dt. \tag{2.31}$$

where  $\Delta^n \hat{\mathcal{H}}$  is the energy-difference function defined in (2.18) for the case of Hamiltonian perturbations and  $y^i(t)$  denotes any of the two unperturbed heteroclinic solutions of system (2.1) <sub>$\epsilon=0$</sub>  connecting the points  $(\bar{x}^0(I_r), I_r, \phi + (i - 1)\Delta\phi)$  and  $(\bar{x}^0(I_r), I_r, \phi + i\Delta\phi)$ .

We will again need to find the zeros of the energy-difference function defined above in order to associate pulse numbers to individual orbits of the reduced dynamics. We define the following zero sets in the annulus  $\hat{A}$ :

$$\begin{aligned} \hat{V}_-^0 &= \emptyset, & \hat{V}_-^n &= \{(\eta, \phi) \in \hat{A} \mid \Delta^n \hat{\mathcal{H}}_D(\phi) = 0\}, & \hat{V}_+^n &= \hat{\mathcal{R}}^n(\hat{V}_-^n), \\ \hat{Z}_-^n &= \{(\eta, \phi) \in V_-^n \mid D_\phi \Delta^n \hat{\mathcal{H}}_D(\phi) \neq 0\}, & \hat{Z}_+^n &= \hat{\mathcal{R}}^n(\hat{Z}_-^n), & n &\geq 1. \end{aligned} \tag{2.32}$$

### 2.3.3. Pulse numbers

For any internal orbit  $\hat{\gamma}$  of the reduced system (2.29) <sub>$\epsilon=0$</sub>  (see Definition 2.4) we can again introduce the *pulse number*

$$N(\hat{\gamma}) = \min\{n \geq 1 \mid \hat{V}_-^k \cap \hat{\gamma} = \emptyset, k = 0, \dots, n - 1, \hat{Z}_-^n \cap \hat{\gamma}\}. \tag{2.33}$$

We will not define the resonant pulse number  $N_R$  for dissipative perturbations, because they only indicate the existence of nontransverse homoclinic orbits to  $\mathcal{A}_\epsilon^R$  in the Hamiltonian limit, which can be destroyed by arbitrarily small dissipative perturbations.

### 2.3.4. Sign sequences

We introduce the following definition:

**Definition 2.5.** Suppose that for an internal orbit  $\hat{\gamma}$  of the reduced system (2.29) <sub>$\epsilon=0$</sub> ,  $N(\hat{\gamma}) \equiv N$  is defined. Then the *positive and negative sign sequences*  $\{\chi^\pm(\hat{\gamma})\}_{k=1}^N$  of  $\hat{\gamma}$  are defined as

$$\begin{aligned} \chi_1^+(\hat{\gamma}) &= +1, \\ \chi_{k+1}^+(\hat{\gamma}) &= \sigma \operatorname{sign}(\Delta^k \hat{\mathcal{H}}|_{\hat{\gamma}}) \chi_k^+(\hat{\gamma}), & k &= 1, \dots, N - 1, \\ \chi_k^-(\hat{\gamma}) &= -\chi_k^+(\hat{\gamma}), & k &= 1, \dots, N - 1, \end{aligned}$$

respectively, with  $\sigma$  defined in (2.26).

2.3.5. *The existence of  $N$ -pulse orbits homoclinic to  $\mathcal{A}_\varepsilon^R$*

We will now present results on multi-pulse orbits connecting the slow manifold  $\mathcal{A}_\varepsilon^R$  to itself. By the possible overflowing or inflowing invariance of  $\mathcal{A}_\varepsilon^R$  these orbits will not necessarily asymptote to slow orbits on  $\mathcal{A}_\varepsilon^R$  in both time directions. Rather, they will approach slow orbits at an exponential rate, as long as the latter orbits stay in the slow manifold in forward or backward time. We will use the following definition:

*Definition 2.6.* We say that an  $N$ -pulse orbit  $y_\varepsilon^N$  of the dissipative system (2.1) *positively approaches* an orbit  $\gamma_\varepsilon^+ \subset \mathcal{A}_\varepsilon$ , if after the  $N$ th pulse solutions on  $y_\varepsilon^N$  approach solutions on  $\gamma_\varepsilon^+$  at an exponential rate, as long as the latter solutions stay in  $\mathcal{A}_\varepsilon^R$ . Similarly, we say that  $y_\varepsilon^N$  *negatively approaches* a slow orbit  $\gamma_\varepsilon^- \subset \mathcal{A}_\varepsilon$ , if  $y_\varepsilon^N$  positively approaches  $\gamma_\varepsilon^- \subset \mathcal{A}_\varepsilon$  in backward time.

We note that if the solutions on  $\gamma_\varepsilon^+$  in the above definition never leave the slow manifold  $\mathcal{A}_\varepsilon^R$  in forward time then “positively approaches” is equivalent to “positively” asymptotic.

Using the quantities defined in Section 2.2, we have the following main result on the multi-pulse behavior in system (2.1) for nonzero dissipation.

*Theorem 2.2.* Assume that hypotheses (H1)–(H5) are satisfied. Suppose that for an internal orbit  $\hat{\gamma}_0^- \subset \hat{A}$  of the reduced system (2.29) $_{\varepsilon=0}$ ,

(A1)  $N \equiv N(\hat{\gamma}_0^-)$  is defined.

(A2) Let  $\hat{b}_- \in \hat{Z}^N \cap \hat{\gamma}_0^-$  and  $\hat{b}_+ = \hat{\mathcal{R}}^N(\hat{b}_-)$ . Assume that the orbit  $\hat{\gamma}_0^+ \subset \hat{A}$  of system (2.29) $_{\varepsilon=0}$  which contains  $\hat{b}_+$  is an internal orbit with  $\hat{Z}_+^N \cap \hat{\gamma}_0^+$ .

Then for each of the two jump sequences  $\{\chi_k^\pm\}$ , there exists  $\varepsilon_0 > 0$  such that for  $0 < \varepsilon < \varepsilon_0$ , the dissipative system (2.1) has an  $N$ -pulse homoclinic orbit  $y_\varepsilon^N$  with jump sequence  $\{\chi_k^\pm\}$  which positively approaches a slow orbit  $\gamma_\varepsilon^+ \subset \mathcal{A}_\varepsilon$  and negatively approaches a slow orbit  $\gamma_\varepsilon^- \subset \mathcal{A}_\varepsilon$ . Moreover, the orbits  $b_\varepsilon \circ g_\varepsilon^{-1}(\gamma_\varepsilon^+)$  and  $\hat{\gamma}_0^+$  are  $(\sqrt{\varepsilon}, C^1)$ -close near  $\hat{b}_-$ , and  $b_\varepsilon \circ g_\varepsilon^{-1}(\gamma_\varepsilon^-)$  and  $\hat{\gamma}_0^+$  are  $(\sqrt{\varepsilon}, C^1)$ -close near  $\hat{b}_+$ .

*Proof.* The main difference in the construction of multi-pulse orbits in the dissipative case is that the unstable manifold  $W^u(\gamma_\varepsilon^-)$  of a slow orbit is not contained in a given three dimensional energy surface any more (see the proof of Theorem 2.1). As a result, we cannot use two-dimensional local and global maps to track solutions as they enter and leave neighborhoods of the slow manifold. Instead, we use three dimensional maps, which are defined in terms of the variables  $(\eta, \phi)$  and the energy of a trajectory upon entering or leaving the neighborhood  $U$  of the slow manifold. From a local analysis near the slow manifold and by Gronwall estimates outside the set  $U$ , we obtain that the  $(\eta, \phi)$  component of the projected global and local maps are still  $C^1$ -close to  $\hat{\mathcal{R}}$  and the identity, respectively. Thus we only have to find approximations for the change of energy along multi-pulse orbits. Careful estimates show (see [15]) that for orbits with a finite number of pulses the change of energy during passages near  $\mathcal{A}_\varepsilon^R$  is smaller in order of magnitude than during global excursions in a vicinity of the unperturbed homoclinic manifolds. The coefficient of the leading order  $\mathcal{O}(\varepsilon)$  term in these global changes of energy is given by the second term in (2.31). Note that the individual terms in this sum do not depend on which of the two unperturbed manifolds the orbit  $y^i(t)$  belongs to. This is a simplification made possible by hypothesis (H5). Using (2.31), an application of the implicit function theorem shows that transverse zeros of  $\Delta^n \mathcal{H}_D$  give rise to  $n$ -pulse homoclinic orbits to the slow manifold  $\mathcal{A}_\varepsilon^R$ . The exact asymptotics of these orbits then can be found by applying Fenichel’s results on the invariant foliations of stable

and unstable manifolds (see, e.g., [34]). This again leads to the definition of the pulse number  $N(\hat{\gamma})$  in (2.33) and proves the statements of the theorem (see Haller and Wiggins [15]).  $\square$

### 3. Multi-pulse orbits in the two-mode truncation of the damped-forced NLS

In this section we return to the two-mode truncation of the damped-forced NLS introduced in Section 1 and investigate the existence of multi-pulse solutions, whose existence is suggested by the numerical experiments of Bishop et al. [3]. It is simple to verify that the mode equations in (1.6) are exactly of the form of system (2.1) with the parameter  $\mu = (\alpha, \beta)$  and with the functions  $H_0, H_1, g_x, g_I$  and  $g_\phi$  defined as follows:

$$H_0 = \frac{1}{2}I^2 - I - \frac{7}{16}x_1^4 - \frac{3}{8}x_1^2x_2^2 + \frac{1}{16}x_2^4 + (I - \frac{1}{2}K^2)x_1^2 - \frac{1}{2}K^2x_2^2, \tag{3.1}$$

$$H_1 = \Gamma\sqrt{2I - x_1^2 - x_2^2} \sin \phi, \tag{3.2}$$

$$\begin{aligned} g_{x_1}(x, I, \phi; \mu, \varepsilon) &= -\beta x_1, & g_I(x, I, \phi; \mu, \varepsilon) &= (\alpha - \beta)(x_1^2 + x_2^2) - 2\alpha, \\ g_{x_2}(x, I, \phi; \mu, \varepsilon) &= -\beta x_2, & g_\phi(x, I, \phi; \mu, \varepsilon) &\equiv 0. \end{aligned} \tag{3.3}$$

Furthermore, easy calculations show that (1.6) $_{\varepsilon=0}^x$  has a hyperbolic fixed point at  $\bar{x}^0(I) = (0, 0)$  with a symmetric pair of homoclinic orbits for any  $I > K^2/2$ . The phase portrait of (1.6) $_{\varepsilon=0}^x$  for such  $I$  values is shown in Fig. 6. (For more details on the unperturbed geometry the reader is referred to Kovačič and Wiggins [24] or Haller and Wiggins [15].) Note that in Fig. 6 we also indicate the direction of the vectors  $\rho(p^+)$  and  $D_x H_0$  which we defined in relation with (2.26) in the previous section. Using (2.26) we immediately obtain

$$\sigma = -1. \tag{3.4}$$

As a result of the geometry shown in Fig. 6, (1.6) satisfies hypothesis (H1) in Section 2.1. Following the discussion in that section, for  $\varepsilon = 0$  we conclude the existence of a two dimensional invariant manifold

$$\mathcal{A}_0 = \{(x, I, \phi) \in \mathcal{P} \mid x = \bar{x}^0(I) = 0, I \in [I_1, I_2], \phi \in S^1\}, \tag{3.5}$$

with  $K^2/2 < I_1 < 1 < I_2$ , and a symmetric pair of three dimensional homoclinic manifolds,  $W_0^+$  and  $W_0^-$  of the type shown in Fig. 1. As a result of the symmetry  $x \mapsto -x$  of (1.6), the invariant manifold  $\mathcal{A}_0 \equiv \mathcal{A}_\varepsilon$  survives the perturbation unchanged. This means that the maps defined in (2.3) and (2.6) take the simple form

$$g_0(I, \phi) \equiv g_\varepsilon(I, \phi) = (0, 0, I, \phi). \tag{3.6}$$

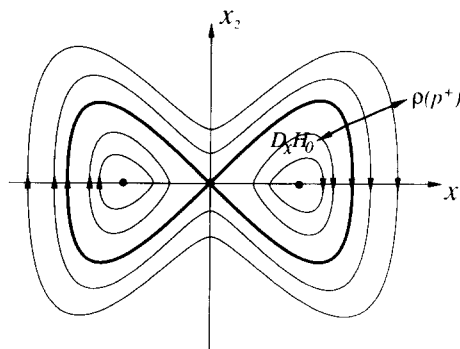


Fig. 6. The phase portrait of (1.6) $_{\varepsilon=0}^x$ .

One can see from (1.6) that  $\mathcal{A}_0$  contains a circle of equilibria,  $C_r$ , satisfying  $I = 1$ . Hence our hypothesis (H2) in Section 2.1 is satisfied for the resonant action value  $I_r = 1$ . From (3.6) we see that the projection map  $\Pi_\varepsilon$  defined in (2.17) is of the simple form  $\Pi_\varepsilon(0, 0, I, \phi) = (\eta, \phi)$ . Recall from Section 2.2.1 that for  $\varepsilon > 0$  this map can be used to blow-up the dynamics on the slow manifold  $\mathcal{A}_\varepsilon^R$  created near  $C_r$ , and project it to the annulus  $\hat{A}$  defined in (2.9).

As seen from the calculations of Kovačič and Wiggins [24], both homoclinic manifolds,  $W_0^+$  and  $W_0^-$ , admit the same constant phase shift

$$\Delta\phi(K) = \begin{cases} 2 \cot^{-1} \left( \frac{K}{\sqrt{2-K^2}} \right) + \frac{2}{\sqrt{7}} \tanh^{-1} \left( \sqrt{\frac{7K^2}{2-K^2}} \right) - \pi, & \text{if } 0 < K < \frac{1}{2}, \\ 2 \tan^{-1} \left( \frac{\sqrt{2-K^2}}{K} \right) + \frac{2}{\sqrt{7}} \tanh^{-1} \left( \sqrt{\frac{2-K^2}{7K^2}} \right), & \text{if } \frac{1}{2} < K < \sqrt{2}. \end{cases} \tag{3.7}$$

Consequently, system (1.6) also satisfies hypothesis (H3) in Section 2.1. A plot of  $\Delta\phi$  as a function of  $K$  can be found in Haller and Wiggins [13]. Here we only note that the range of  $\Delta\phi(K)$  is  $[0, +\infty)$ .

Based on the above observations, the two-mode model (1.6) is an ideal candidate for the application of the energy-phase method described in Section 2. Our main goal will be to find multi-pulse homoclinic behavior in this model in the sense of Definition 2.1. First, we consider the purely Hamiltonian undamped-forced system ( $\alpha = \beta = 0$ ), then study the damped-forced equations with  $\alpha, \beta > 0$ .

### 3.1. The forced two-mode model ( $\alpha = \beta = 0$ )

We will now compute all the ingredients which are necessary for the application of the energy-phase method described in Section 2.2.

#### 3.1.1. Energy-difference functions and their zeros

As we discussed in Section 2.2.1, the projection map  $\Pi_\varepsilon$  can be used to approximate the slow orbits in  $\mathcal{A}_\varepsilon^R$  by the level curves of the reduced Hamiltonian defined in (2.15). For our two-mode problem we easily obtain

$$\hat{\mathcal{H}}(\eta, \phi) = \frac{1}{2}\eta^2 + \sqrt{2}\Gamma \sin \phi, \tag{3.8}$$

defined on  $(\hat{A}, \hat{\omega})$  with some

$$\eta_0 > \tilde{\eta} = 2\sqrt{\sqrt{2}\Gamma}. \tag{3.9}$$

Fig. 7 shows the level curves of  $\hat{\mathcal{H}}$  and explains our choice of  $\eta_0$  in (3.9) to include all the internal orbits associated with the presence of the resonance (see Definition 2.2). Note that the phase portrait of the reduced Hamiltonian is just that of the ordinary pendulum shifted by  $-\pi/2$  in  $\phi$ . As shown in Fig. 7, we denote the open domain enclosed by the heteroclinic cycle of the pendulum by  $\hat{S}_0$ . Note that the two elements of this cycle are in fact homoclinic orbits since they are asymptotic to the same point in forward and backward time. As a result, all orbits in  $\hat{A}$ , with the exception of the saddle and the center, are internal orbits by Definition 2.2.

Using (2.18) and (3.8) we have the  $n$ th order energy-difference function of the form

$$\Delta^n \hat{\mathcal{H}}(\phi) = \sqrt{2}\Gamma [\sin(\phi + n\Delta\phi) - \sin \phi]. \tag{3.10}$$

From (3.10) we obtain that for any  $n$  satisfying

$$n\Delta\phi \neq 2l\pi, \quad l \in \mathbb{Z}, \tag{3.11}$$

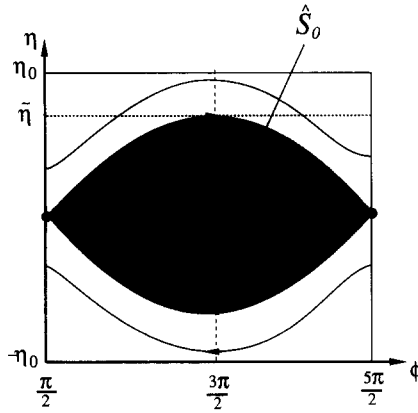


Fig. 7. The phase portrait of the reduced Hamiltonian  $\hat{\mathcal{H}}$ .

the zeros of  $\Delta^n \hat{\mathcal{H}}$  in  $[\pi/2, 5\pi/2]$  are

$$\phi_{-,1}^n = \frac{5}{2}\pi - \frac{1}{2}n\Delta\phi \bmod 2\pi, \quad \phi_{-,2}^n = \frac{5}{2}\pi - [\pi + \frac{1}{2}n\Delta\phi] \bmod 2\pi. \quad (3.12)$$

Both zeros are transverse under the condition (3.11). Introducing the two additional angles

$$\phi_{+,1}^n = [\phi_{-,1}^n + n\Delta\phi] \bmod 2\pi, \quad \phi_{+,2}^n = [\phi_{-,2}^n + n\Delta\phi] \bmod 2\pi, \quad (3.13)$$

and using the definitions of the zero sets in (2.19)–(2.21), we obtain

$$\begin{aligned} \hat{Z}_-^n &= \hat{Z}_-^n = \left\{ (\eta, \phi) \in \hat{A} \mid \phi \in \{\phi_{-,1}^n, \phi_{-,2}^n\} \right\}, \\ \hat{Z}_+^n &= \hat{Z}_+^n = \left\{ (\eta, \phi) \in \hat{A} \mid \phi \in \{\phi_{+,1}^n, \phi_{+,2}^n\} \right\}. \end{aligned} \quad (3.14)$$

Notice that  $\hat{Z}_-^n$  and  $\hat{Z}_+^n$  are symmetric with respect to the line  $\phi = \frac{3}{2}\pi$ , which contains the center shown in Fig. 7. This has the important consequence that  $\hat{\gamma}_0^- = \hat{\gamma}_0^+$  will hold for a periodic orbit  $\hat{\gamma}_0^-$  satisfying the assumptions of Theorem 2.1, leading to *homoclinic*  $N$ -pulse orbits in all cases.

### 3.1.2. Pulse numbers

Note that under (3.11) all periodic internal orbits outside  $\hat{S}_0$  intersect  $\hat{Z}_-^1$  transversally (see Fig. 7). Hence, for any periodic or homoclinic orbit  $\hat{\gamma}$  outside  $\hat{S}_0$  the pulse number defined in (2.23) is  $N(\hat{\gamma}) = 1$ . We will now classify the periodic orbits within  $\hat{S}_0$  based on their pulse numbers using a geometric construction.

Let us start by defining the energy sequence

$$\hat{h}_0 = \sqrt{2}\Gamma, \quad \hat{h}_n = \min(\hat{\mathcal{H}}(0, \phi_{-,1}^n), \hat{\mathcal{H}}(0, \phi_{-,2}^n)), \quad (3.15)$$

and the sequence of sets

$$\hat{A}_0 = \emptyset, \quad \hat{A}_n = \{(\eta, \phi) \in \hat{S}_0 \mid \hat{\mathcal{H}}(\eta, \phi) > \hat{h}_n\}, \quad n \geq 1. \quad (3.16)$$

For  $n \geq 1$   $\hat{A}_n$  has the following simple meaning: it is the open set of internal orbits in  $\hat{S}_0$  which intersect at least one component of  $\hat{Z}_-^n$  transversally (see Fig. 8a). We note that the element  $\hat{h}_n$  of the energy sequence in (3.15) gives the reduced energy of the periodic orbit  $\hat{\gamma}_n$  which is the inner boundary of  $\hat{A}_n$ . Next, we extract

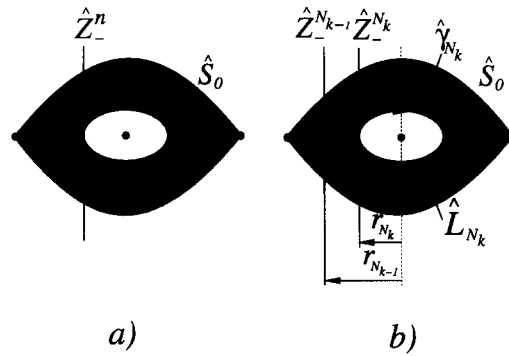


Fig. 8. The construction of the layer sequence.

the maximal decreasing subsequence of the energy sequence and arrange the indices in this subsequence into a *pulse sequence*,  $N_k$ . More precisely, we define the pulse sequence as

$$N_1 = 1, \quad N_k = \min\{n \in \mathbb{Z}^+ | n > N_{k-1}, \hat{h}_n < \hat{h}_{N_{k-1}}\}, \quad k \geq 2. \tag{3.17}$$

Since the energy of the periodic orbits in  $\hat{S}_0$  decreases monotonically as they shrink to the center, we must necessarily have

$$\hat{A}_{N_1} \subset \hat{A}_{N_2} \subset \dots \subset \hat{A}_{N_k} \subset \dots$$

This sequence of sets is infinite if the condition (3.11) is satisfied for all  $n \in \mathbb{Z}$ . If, however,  $m$  is the minimal index such that  $N_m \Delta \phi = 2l\pi$  occurs for some integer  $l$ , then the pulse sequence and the set sequence  $\{\hat{A}_{N_k}\}$  are finite and have  $m$  elements, with  $\hat{A}_{N_m} \equiv \hat{S}_0$ . In both cases we can define the finite or infinite *layer sequence*

$$\hat{L}_{N_k} = \text{Int}(\hat{A}_{N_k} \setminus \hat{A}_{N_{k-1}}), \tag{3.18}$$

where  $\text{Int}(\cdot)$  refers to the interior of a set. The construction of the layer sequence is shown in Fig. 8b. Note that  $\hat{L}_{N_k}$  is an open set and its inner boundary is the unique periodic orbit  $\hat{\gamma}_{N_k}$  in  $\hat{S}_0$  with

$$\mathcal{H}|\hat{\gamma}_{N_k} = \hat{h}_{N_k}. \tag{3.19}$$

Hence, as shown in Fig. 8b, the “half-width” of the periodic orbit  $\hat{\gamma}_{N_k}$  is the inner angular radius of the layer  $\hat{L}_{N_k}$ , and it equals

$$r_{N_k} = \min(|\frac{3}{2}\pi - \phi_{-1}^{N_k}|, |\frac{3}{2}\pi - \phi_{-2}^{N_k}|). \tag{3.20}$$

The significance of the whole construction in this subsection lies in the following observation: if the pulse sequence is infinite, then no periodic orbit  $\hat{\gamma} \subset \hat{L}_{N_k}$  intersects  $\hat{V}_-^n = \hat{Z}_-^n$  for  $n < N_k$ , but each of them intersects  $\hat{Z}_-^{N_k}$  transversally. If the pulse sequence is finite, i.e., it terminates at an index  $N_m \geq 1$ , then a periodic orbit  $\hat{\gamma} \subset \hat{L}_{N_k}$  does not intersect  $\hat{V}_-^n = \hat{Z}_-^n$  for  $n < N_k < N_m$  but it intersects  $\hat{Z}_-^{N_k}$  transversally. Since in the latter case condition (3.11) is violated for  $n = N_m$ , we have  $\hat{V}_-^{N_m} \equiv \hat{A}$  and  $\hat{Z}_-^{N_m} = \emptyset$ . Also note that any “boundary orbit”  $\hat{\gamma}_{N_k}$  has no intersection with  $\hat{Z}_-^n$  for  $n < N_k$ , but it is tangent to  $\hat{Z}_-^{N_k}$ . Based on the definition of pulse numbers in (2.23) and (2.24), we have obtained the following result.

*Proposition 3.1.* If condition (3.11) holds for all  $n \geq 1$  (i.e., the pulse sequence is infinite), then for any periodic orbit  $\hat{\gamma} \subset \hat{L}_{N_k}$  we have  $N(\hat{\gamma}) = N_k$ . On the other hand, if  $\bar{n} \geq 1$  is the minimal integer for which (3.11) is violated (i.e., the pulse sequence terminates at  $N_m = \bar{n}$ ), then for any periodic orbit  $\hat{\gamma} \subset \hat{L}_{N_k}$ ,  $k < m$ ,

we have  $N(\hat{\gamma}) = N_k$ . Furthermore, for any periodic orbit  $\hat{\gamma} \in \hat{L}_{N_m}$  we have  $N_R(\hat{\gamma}) = N_m = \bar{n}$ . Finally, for the boundary orbits  $\hat{\gamma}_{N_k}$  the pulse numbers  $N(\hat{\gamma}_{N_k})$  and  $N_R(\hat{\gamma}_{N_k})$  are not defined.

Notice that, with the exception of the boundary orbits  $\hat{\gamma}_{N_k}$ , we have formally computed the pulse numbers of all internal orbits lying in the pendulum domain  $\hat{S}_0$ . Based on Theorem 2.1, each layer  $\hat{L}_{N_k}$  of periodic orbits indicates a layer of slow periodic orbits on the manifold  $\mathcal{A}_\varepsilon^R$  with its  $\Pi_\varepsilon$ -projection close to  $\hat{L}_{N_k}$ , such that each slow orbit in the layer admits (at least) two  $N_k$ -pulse homoclinic orbits. Before we elaborate on the exact number and shape of these multi-pulse orbits, we will give a more concrete description of the pulse sequences and layers we have constructed recursively.

To demonstrate the dependence of the pulse sequence (3.17) on the parameters, we chose to vary  $\Delta\phi$  instead of  $k$  (one can relate these two parameters using (3.7)). In Figs. 9a–c we plotted the pulse sequence as a function of the phase shift  $\Delta\phi$ . We chose 500, 100, and 10, respectively, as upper bounds on the pulse numbers. By definition, each point  $(\Delta\phi, N_k)$  of this diagram indicates the existence of an infinite number of internal orbits with pulse number  $N_k$  for the given parameter value  $\Delta\phi$ . These plots show a stable pulse-distribution for low pulses but show an increasing sensitivity of higher and higher pulses to small changes in the phase shift. Note that while single-pulse orbits exist for all parameter values, there seems to be no general rule describing possible higher-pulse connections. Rather, an infinite number of combinations of subsequent pulse numbers are possible and they are all realized as the phase shift varies from 0 to  $2\pi$ . It is important to point out, however, that for finite values of  $\varepsilon$  one has to cut off these plots at some finite pulse number, because the methods used in the proof of Theorem 2.1 do not work for orbits arbitrarily close to the center in Fig. 6. Still, the meaningful part of the pulse-diagram and so the number of distinct pulse-sequences tends to infinity as  $\varepsilon \rightarrow 0$ .

As an alternative characterization of the layer structure on the slow manifold  $\mathcal{A}_\varepsilon^R$ , one can plot how the layer radius sequence defined in (3.20) varies with the parameter  $\Delta\phi$ . To construct this plot, we first observe that the periodic orbit  $\hat{\gamma}_{N_k}$  has the following property: its image under the map  $\mathcal{R}^{N_k}$  (see (2.11)) is tangent to  $\hat{\gamma}_{N_k}$  itself, and  $N_k$  is the minimal positive integer for which this tangency occurs. A simple calculation yields that, in general,  $\hat{\mathcal{R}}^N(\hat{\gamma})$  is tangent to  $\hat{\gamma}$ , if the angular radius  $r_N$  of  $\hat{\gamma}$  satisfies the relation

$$r_N = |l\pi - \frac{1}{2}N\Delta\phi| \tag{3.21}$$

for some integer  $l$ . Then, looking at the steps leading to Proposition 3.1, one finds that the construction of the layer sequence is equivalent to the following construction of layer radii: **1.** Select  $N = 1$  and consider the two one-parameter families of lines on the  $(r, \Delta\phi)$  parameter space given by (3.21). **2.** Keeping in mind that the maximal meaningful value of  $r$  is  $\pi$  and restricting  $\Delta\phi$  to  $[0, 2\pi]$ , find the line segments from the above families within the rectangle  $[0, \pi] \times [0, 2\pi]$  which are the closest to the  $\Delta\phi$  axis. This gives a tent-like object, as shown in Fig. 10a, which shows how the inner angular radius  $r_1$  of the layer  $\hat{L}_1$  changes with  $\Delta\phi$ . **3.** Next, set  $N = 2$  and consider the line segments from the families in (3.21) which lie below the  $\hat{L}_1$  tent and are the closest to the  $\Delta\phi$  axis. As shown in Fig. 10b, this time we obtain an “inverse” tent, which we will call  $\hat{L}_2$ -tent. Once again, the  $\hat{L}_2$ -tent shows how the inner radius  $r_2$  of the  $\hat{L}_2$  layer, if it exists at all, changes as  $\Delta\phi$  varies. **4.** Repeat the above construction recursively: always increase the integer  $N$  by one and define the  $\hat{L}_{N+1}$  tent to be the line segments from the families (3.21) which lie below all previous tents and are the closest to the  $\Delta\phi$  axis (see Fig. 10a for  $N = 3$  and Fig. 10b for  $N = 4$ ).

The diagram obtained this way can, in principle, be constructed up to arbitrary high indices by hand, but it is best to implement the simple algorithm leading to the layer radius sequence (3.20) on a computer. We obtained Fig. 11 in this manner, which shows the union of all  $\hat{L}_N$ -tents for  $N \leq 100$ . By definition, for any fixed value of the phase shift the points of the diagram above this value show the inner angular radii for the layers  $\hat{L}_{N_k}$  with  $N_k \leq 100$ . The resulting plot approaches an infinite binary tree as  $N \rightarrow \infty$ , so we will refer to

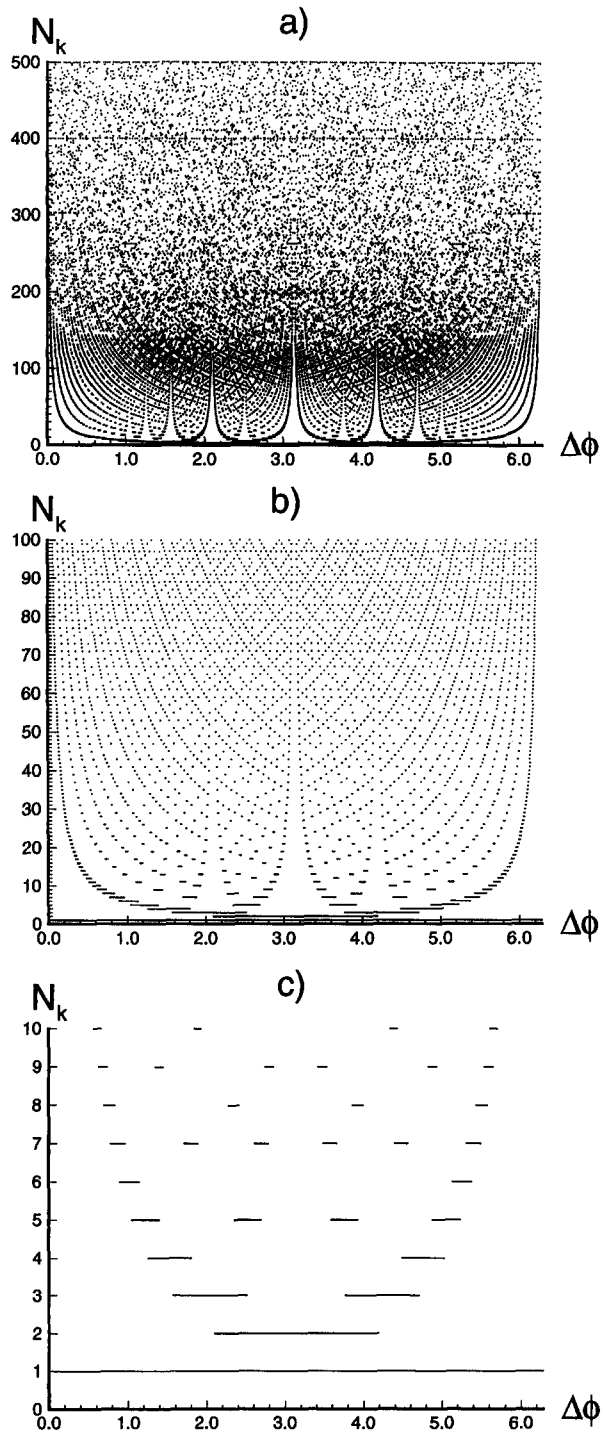


Fig. 9. The pulse sequence as a function of the phase shift.

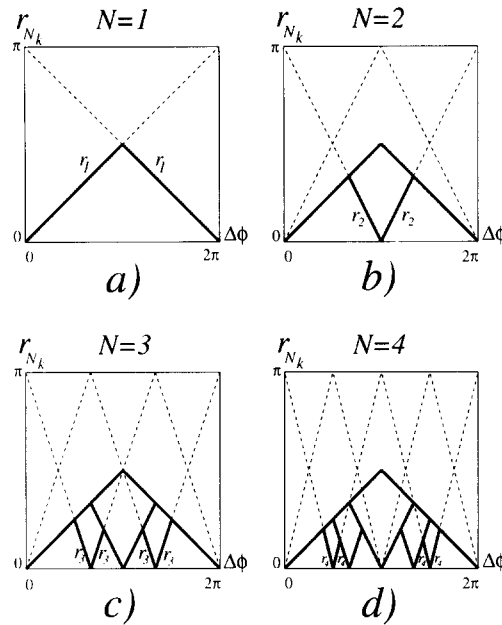


Fig. 10. The graphical construction of layer radii as a function of the phase shift.

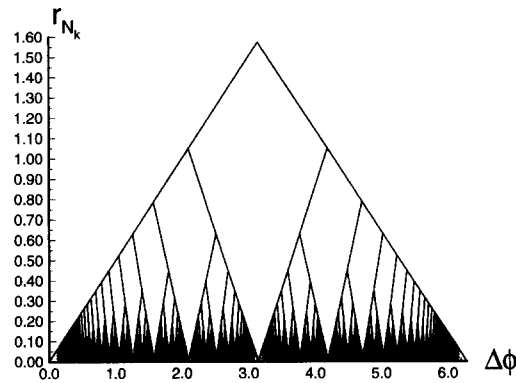


Fig. 11. The layer radius sequence as a function of the phase shift.

the structure shown in Fig. 11 as the *homoclinic tree* in the limit  $N \rightarrow \infty$ . At the branching points one of the layers bifurcates to two new layers with different pulse numbers. As for any binary tree, the set of branching points forms a countable set as  $N$  tends to infinity. As we discussed in connection with the pulse sequence plotted in Fig. 9, the homoclinic bifurcations that occur on this set of parameters do not necessarily double or triple the value of  $N$ . We finally note that the homoclinic tree intersects the  $\Delta\phi$  axis at the values of  $\Delta\phi$  where condition (3.11) is violated for some  $n$  and  $l$ . These points indicate degenerate layers of slow periodic orbits for which only the resonant pulse number  $N_R$  is defined.

### 3.1.3. Jump sequences

In this section we compute the sign sequences introduced in Section 2.4.4. As one can see from (i) of Theorem 2.1, these sequences can be used to describe the shape of the  $N$ -pulse homoclinic orbits we found above.

Suppose that for some internal orbit  $\hat{\gamma}_0^- \subset \hat{S}_0$  the pulse number  $N(\hat{\gamma}_0^-) \equiv N > 1$  is defined. Then from (2.23) we obtain that for  $k = 1, \dots, N - 1$   $\hat{\mathcal{R}}^k(\hat{\gamma}_0^-)$  does not intersect any orbit with reduced energy  $\hat{\mathcal{H}}|\hat{\gamma}_0^-$ . In particular, it does not intersect  $\hat{\gamma}_0^-$  itself. Since  $\hat{\mathcal{R}}$  preserves area, this means that  $\hat{\mathcal{R}}^k(\hat{\gamma}_0^-)$  lies outside the domain encircled by  $\hat{\gamma}_0^-$ . But all orbits outside  $\hat{\gamma}_0^-$  have energies higher than  $\hat{\gamma}_0^-$ ; hence the value of the reduced Hamiltonian  $\hat{\mathcal{H}}$  at any point of  $\hat{\mathcal{R}}^k(\hat{\gamma}_0^-)$  will be higher than  $\hat{\mathcal{H}}|\hat{\gamma}_0^-$  for  $k = 1, \dots, N - 1$ . Therefore, we have

$$\text{sign}(\hat{\mathcal{H}}|\hat{\mathcal{R}}^k(\hat{\gamma}_0^-) - \hat{\mathcal{H}}|\hat{\gamma}_0^-) = +1, \quad k = 1, \dots, N - 1.$$

Using this, (3.4), and the definition of the positive and negative sign sequences in Definition 2.3 we obtain

$$\chi^+(\hat{\gamma}_0^-) = \{+1, -1, +1, -1, \dots\}, \quad \chi^-(\hat{\gamma}_0^-) = \{-1, +1, -1, +1, \dots\}. \quad (3.22)$$

According to (i) of Theorem 2.1 and Definition 2.1, this means that the multi-pulse orbits constructed in the previous section always jump from the neighborhood of one unperturbed homoclinic structure to the other. The same argument shows that for  $N = N_R$  the jump sequences are also alternating.

### 3.1.4. Multi-pulse orbits

As we have seen, for any element  $N_k$  of the pulse sequence which satisfies the nonresonance condition (3.11) we can guarantee the existence of transverse  $N_k$ -pulse orbits with alternating jump sequences, which are doubly asymptotic to the slow manifold  $\mathcal{A}_\varepsilon^R$ . Most of these orbits will be homoclinic to slow periodic solutions, which either lie inside or outside the domain  $\hat{S}_0$ . In the latter case the corresponding homoclinic orbits are all 1-pulse orbits, and each periodic orbit admits four such homoclinic orbits since the corresponding internal orbits outside  $\hat{S}_0$  intersect both components of the zero set  $\hat{Z}_-^1$  transversally (see Haller and Wiggins [13] for a discussion on such orbits). The internal orbits lying inside  $\hat{S}_0$  within some layer  $\hat{L}_{N_k}$  have two distinct intersections with the component of  $\hat{Z}_{N_k}^1$  which lies closer to the center at  $\phi = \frac{3}{2}\pi$ . As a result, the corresponding slow periodic orbits on  $\mathcal{A}_\varepsilon^R$  admit four transverse homoclinic orbits (see Haller and Wiggins [13] for illustration). A sub-layer  $\hat{L}_{1,1}$  of  $\hat{L}_1$  is exceptional, because it contains internal orbits intersecting both components of  $\hat{Z}_1^N$ . Consequently, the corresponding slow periodic orbits on  $\mathcal{A}_\varepsilon^R$  admit eight transverse homoclinic orbits. Finally, any layer  $\hat{L}_{N_k}$  with  $N_k > 1$  indicates a set of periodic orbits on the slow manifold  $\mathcal{A}_\varepsilon^R$  which admit four transverse,  $N_k$ -pulse solutions with alternating jump sequences (see Fig. 12 for an illustration for the case  $N_2 = 2$ ).

Since, as mentioned in Section 5.1.3, the pulse number of the separatrices forming the boundary of  $\partial\hat{S}_0$  equals one, and the separatrices intersect both components of  $Z_-^1$ , Theorem 2.1 implies the existence of four transverse 1-pulse orbits homoclinic to the two saddle-saddle fixed points (see Haller and Wiggins [13] for a derivation and illustration of this result using a Melnikov-type method). We now summarize our main results for the forced, undamped two-mode model of the NLS in the following theorem.

**Theorem 3.1.** For some fixed value of the parameter  $\Delta\phi$  let us consider the pulse sequence defined in (3.17) and plotted as a function of  $\Delta\phi$  in Figs. 9a–c. Then for any element  $N_k$  of this sequence satisfying (3.11) there exists  $\varepsilon_0(\mu, N_k) > 0$  such that for  $0 < \varepsilon < \varepsilon_0(N_k)$

(i) System (1.6) (with  $\alpha = \beta = 0$ ) has an infinite number of transverse  $N_k$ -pulse orbits homoclinic to slow periodic solutions on the manifold  $\mathcal{A}_\varepsilon^R$  (see Fig. 12 for  $N_k = 2$ ). Accordingly, there exist Smale horseshoes on the energy levels containing these orbits. Each such slow periodic orbit in these level sets has in fact two transverse  $N_k$ -pulse homoclinic orbits with the jump sequence  $+1, -1, \dots$  and two with the jump sequence  $-1, +1, \dots$

(ii) The slow periodic orbits with transverse  $N_k$ -pulse orbits form a smooth layer  $L_{N_k}^\varepsilon$  on  $\mathcal{A}_\varepsilon^R$  which is  $C^1$   $\sqrt{\varepsilon}$ -close to  $\Pi_\varepsilon^{-1}(\hat{L}_{N_k})$ . A subset of  $L_1^\varepsilon$  contains slow periodic orbits with eight 1-pulse homoclinic orbits.

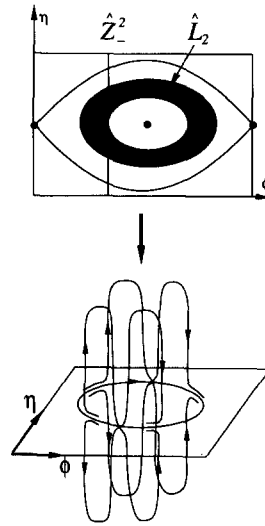


Fig. 12. Double-pulse orbits homoclinic to slow periodic orbits.

(iii) For  $N_k = 1$  there also exist four transverse 1-pulse transverse homoclinic orbits saddle-saddle-type equilibrium.

If  $N_k$  does not satisfy condition (3.11) then the above statements still hold with the exception of transversality and the existence of Smale horseshoes.

To illustrate the statements of Theorem 3.1 numerically, we first selected the parameter values  $k = 0.65$  and  $\Gamma = 1.0$ . Then one obtains from (3.7) that the value of the phase shift is  $\Delta\phi = 2.8890$ . As one can verify from the pulse diagrams in Figs. 9a–c, for this value of the phase shift the first four elements of the pulse sequence are:  $N_1 = 1$ ,  $N_2 = 2$ ,  $N_3 = 11$ , and  $N_4 = 24$ . The corresponding inner angular radii for the first four elements of the layer sequence in (3.18) can be computed to equal  $r_1 = 1.4445$ ,  $r_2 = 0.2525$ ,  $r_{11} = 0.1818$ , and  $r_{24} = 0.1111$  (see also (3.20)). Based on (i), (ii) of Theorem 3.1, there exists a smooth layer  $L_2^\varepsilon \subset \mathcal{A}_\varepsilon^R$  such that each periodic orbit in  $L_2^\varepsilon$  has two 2-pulse homoclinic orbits for both possible alternating jump sequences. We selected a periodic orbit  $\hat{\gamma}_0 \subset \hat{L}_2$  of  $\hat{\mathcal{H}}$  as shown in the upper right hand corner of Fig. 13. The figure also shows the location of the zero sets  $\hat{Z}_-^2$  and  $\hat{Z}_+^2$  in  $\hat{A}$ . We then located a slow periodic orbit  $\gamma_\varepsilon$  on  $\mathcal{A}_\varepsilon^R$  which projects  $C^1$   $\sqrt{\varepsilon}$ -close to  $\hat{\gamma}_0$  under the map  $\Pi_\varepsilon$ ; hence it must fall in  $L_2^\varepsilon$ . To find a 2-pulse orbit homoclinic to  $\gamma_\varepsilon$  with jump sequence  $\{+1, -1\}$ , we followed the component of the unstable manifold of  $\gamma_\varepsilon$  which lies near the unperturbed homoclinic manifold  $W_0^+$ . We also iterated a part of the stable manifold of  $\gamma_\varepsilon$  which lies near the unperturbed homoclinic manifold  $W_0^-$ . The results are projected on the  $(x_1, \eta, \phi)$  coordinate space. As Fig. 13 shows, the two invariant manifolds intersect in a fashion predicted by Theorem 3.1, giving rise to two transverse double-pulse homoclinic orbits. We also show the “shadowing set”  $Y^{2+}$  of unperturbed heteroclinic orbits which appear in Definition 2.1. By the symmetry  $x \mapsto -x$  of the two-mode model (1.6), these numerical results imply the existence of another pair of homoclinic orbits with opposite jump sequence, as predicted by Theorem 3.1. Fig. 14 shows the numerical construction of a 3-pulse jumping orbit predicted by Theorem 3.1. Here the parameter values are  $k = \Gamma = 1.$ , which yield the phase shift  $\Delta\phi = 1.8714$ . This time the first four elements of the pulse sequence are  $N_1 = 1$ ,  $N_2 = 3$ ,  $N_3 = 7$ , and  $N_4 = 10$ . The corresponding inner angular radii are  $r_1 = 0.9357$ ,  $r_3 = 0.3345$ ,  $r_7 = 0.2668$ , and  $r_{10} = 0.0677$  (see also (3.20)). The selected internal orbit  $\hat{\gamma}_0$  from the layer  $\hat{L}_3$  is shown in the upper right hand corner of the figure, and the global unstable and local

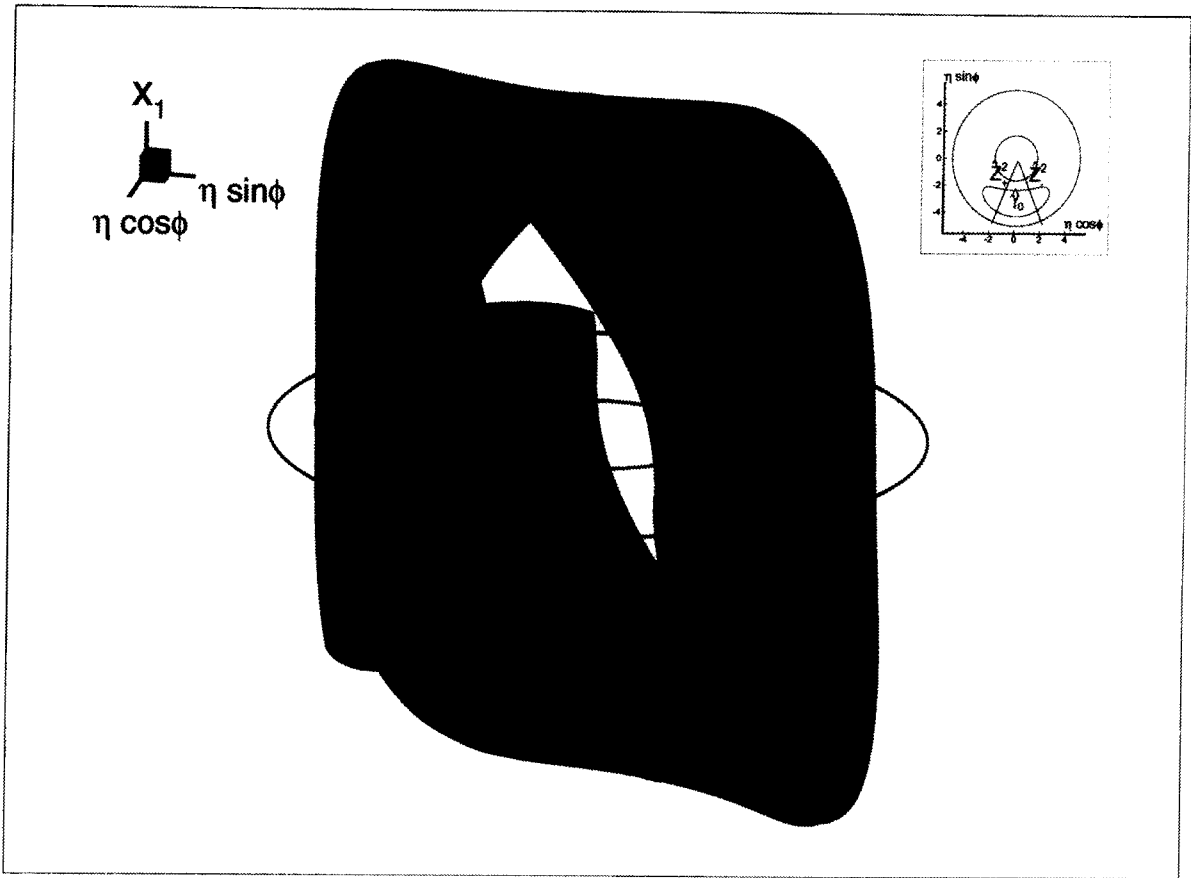


Fig. 13. Double-pulse homoclinic orbit ( $\epsilon = 10^{-4}$ , stepsize =  $1 \times 10^{-4}$ , integrationtime = 16.0).

stable manifolds of a nearby slow periodic orbit are followed numerically to find a 3-pulse homoclinic orbit with jump sequence  $\{+1, -1, +1\}$ . Again, the shadowing set  $Y^{3+}$  of unperturbed orbits is also plotted in the figure.

Note that the transverse intersection of the two invariant manifolds indicated by the projection is real, since on a fixed small tube around  $\mathcal{A}_\epsilon^R$   $D_{x_2}H \neq 0$ ; hence the energy surface is locally a graph over the  $(x_1, \eta, \phi)$  variables. However, the self-intersections of the stable manifolds in the figures are of course artifacts of the projections from the four dimensional phase space. To show this, we plotted a “four dimensional” image in Fig. 15 for the intersection of the stable and unstable manifolds of a slow periodic orbit admitting 1-pulse homoclinic orbits. The parameter values here are again  $k = 0.65$ ,  $\Gamma = 1.$ , so the value of the phase shift, as well as the pulse sequence and layer radius sequence are the same as in our first numerical experiment. This time, however, we color-coded the stable and unstable manifolds of the slow periodic orbit according to the value of the fourth coordinate (i.e.,  $x_2$ ) at its points. Notice, that along the apparent self-intersection of the unstable manifold the limits of the colors are significantly different (see also the color table in the figure). This confirms that the invariant surface does not intersect in the four dimensional phase space.

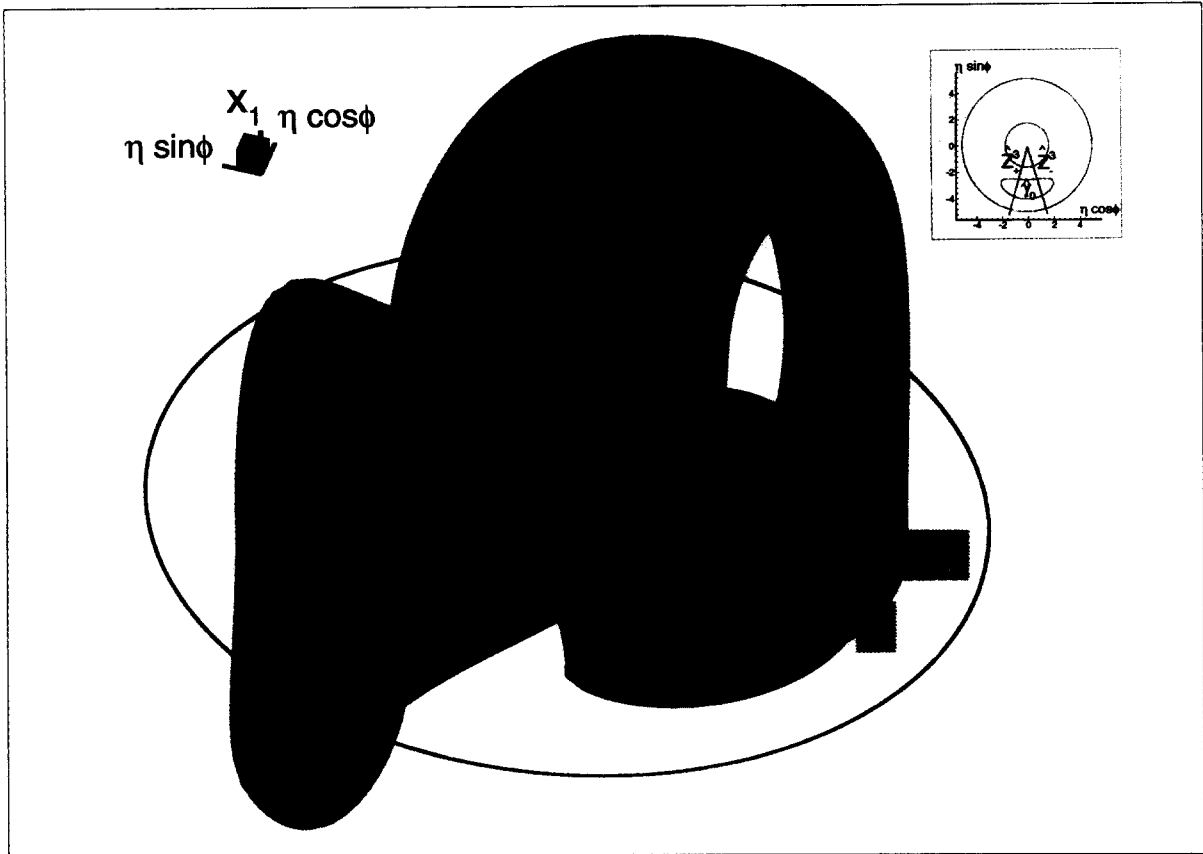


Fig. 14. Triple-pulse homoclinic orbit ( $\epsilon = 10^{-4}$ , stepsize =  $1 \times 10^{-4}$ , integrationtime = 22.3).

### 3.2. The forced-damped two-mode model ( $\alpha, \beta \neq 0$ )

In this section we study the multi-pulse behavior in system (1.6) for nonzero damping. This includes the special case of mode independent damping  $\alpha = \beta$  which was studied numerically by Bishop et al. [2].

First we note that from (3.3) we obtain that

$$D_I g_I(\bar{x}^0(I_r), I_r, \phi; 0) + D_\phi g_\phi(\bar{x}^0(I_r), I_r, \phi; 0) = -2\alpha,$$

hence hypothesis (H4) of Section 2.3.1 is satisfied for  $\alpha > 0$ . Furthermore, (3.2) and (3.3) together yield

$$\langle DH_0, g \rangle|_{I=I_r} = (\alpha + \frac{3}{4}\beta)x_1^4 + (\alpha + \frac{1}{2}\beta)x_1^2x_2^2 + 2[\beta(1 - \frac{1}{2}K^2) - \alpha]x_1^2 + \beta(K^2 - \frac{1}{4})x_2^2.$$

Since this expression is even in both  $x_1$  and  $x_2$ , and for the unperturbed homoclinic orbits we have  $x^{h+}(t, I_r) = -x^{h-}(t, I_r)$ , hypothesis (H5) of Section 2.3.1 is also satisfied.

#### 3.2.1. The dissipative reduced system

As we noted in Section 2.3.1, for  $\epsilon > 0$  sufficiently small compact pieces of the orbits on the slow manifold  $\mathcal{A}_\epsilon^R$  can be approximated by the dissipative reduced system (2.29) provided the nondegeneracy condition (H5) holds. Here the dissipative reduced system (2.29) takes the concrete form

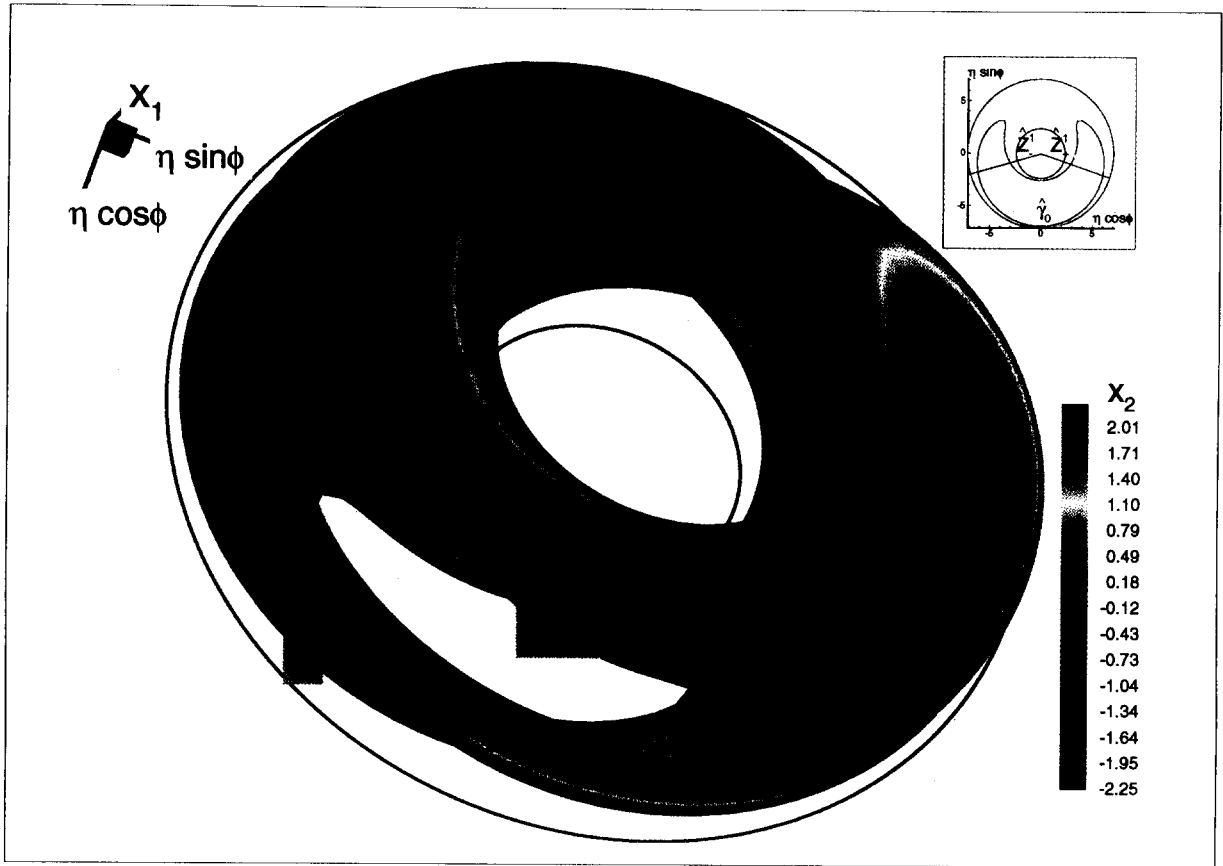


Fig. 15. Single-pulse homoclinic orbit ( $\varepsilon = 10^{-4}$ , stepsize =  $8 \times 10^{-5}$ , integration time = 11.0).

$$\begin{aligned} \dot{\eta} &= -\sqrt{2}\Gamma \cos \phi - 2\alpha - \sqrt{\varepsilon}2\alpha\eta, \\ \dot{\phi} &= \eta. \end{aligned} \tag{3.23}$$

Recall that for  $\varepsilon = 0$  this is a locally Hamiltonian system that can be derived from the function

$$\hat{\mathcal{H}}_D(\eta, \phi; \mu_0) = \frac{1}{2}\eta^2 + \sqrt{2}\Gamma \sin \phi + 2\alpha\phi, \tag{3.24}$$

which we computed using (2.30).

We will restrict the analysis to the nontrivial case when

$$0 < \frac{\sqrt{2}\alpha}{|\Gamma|} < 1, \tag{3.25}$$

holds, in which case (3.23) $_{\varepsilon=0}$  has a center and a saddle in its phase portrait, as shown in Fig. 16a. The center,  $\hat{p}_c$ , and the saddle,  $\hat{p}_s$ , are located at the points

$$(\eta_c, \phi_c) = (0, \pi + \cos^{-1}(\sqrt{2}\zeta)), \quad (\eta_s, \phi_s) = (0, \pi - \cos^{-1}(\sqrt{2}\zeta)), \tag{3.26}$$

respectively, with  $\zeta = \alpha/\Gamma$ . To incorporate the whole domain,  $\hat{S}_\zeta$ , bounded by the orbit homoclinic to the saddle in our study, we define the blown-up annulus  $\hat{A}$  with some  $\eta_0$  satisfying

$$\eta_0 > \tilde{\eta} = 2\sqrt{\sqrt{2}\Gamma(\Gamma - 2\alpha^2) + \alpha[\pi - \cos^{-1}(\sqrt{2}\alpha/\Gamma)]},$$

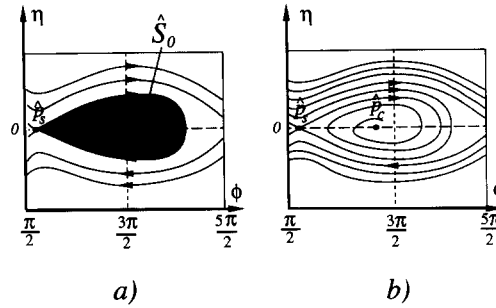


Fig. 16. The phase portrait of the dissipative reduced system.

in accordance with Fig. 16a. For  $\varepsilon > 0$  the forced pendulum-type phase portrait of (3.23) changes into a dissipative one shown in Fig. 16b. Note that the locations of the two equilibria do not change, but  $p_c$  becomes a sink and  $p_s$  becomes a saddle whose eigenvalues add up to a small negative number.

### 3.2.2. Energy-difference functions and their zeros

As we have seen in Section 2.3, the first step in locating multi-pulse homoclinic orbits to  $\mathcal{A}_\varepsilon^R$  is to identify the zero sets of the (dissipative)  $n$ th order energy-difference function (2.31) which now takes the form

$$\Delta^n \hat{\mathcal{H}}_D(\phi; \mu_0) = \sqrt{2}\Gamma[\sin(\phi + n\Delta\phi) - \sin v] - n \int_{-\infty}^{\infty} \langle DH_0, g \rangle|_{y(t)} dt, \tag{3.27}$$

where we used the fact that all elements in the sum of integrals in (2.31) are equal. Using the form of the unperturbed vector field and the calculations of Kovačič and Wiggins [24], we can write

$$\begin{aligned} C(\alpha, \beta, K) &\equiv \int_{-\infty}^{\infty} \langle DH_0, g \rangle|_{y(t)} dt = \int_{-\infty}^{\infty} [-2\alpha\dot{\phi} + (\alpha - \beta)(x_1^2 + x_2^2)\dot{\phi} + \beta(x_1\dot{x}_2 + x_2\dot{x}_1)] dt \\ &= -8\alpha K^2 \Delta\psi(K) + (\alpha - \beta) \cdot \frac{8}{7} [K\sqrt{2 - K^2} + (1 + 3K^2)\Delta\psi(K)], \end{aligned} \tag{3.28}$$

where

$$\Delta\psi(K) = \begin{cases} -\frac{2}{\sqrt{7}} \tanh^{-1} \sqrt{\frac{7K^2}{2 - K^2}}, & \text{if } 0 < K < \frac{1}{2}, \\ -\frac{2}{\sqrt{7}} \tanh^{-1} \sqrt{\frac{2 - K^2}{7K^2}}, & \text{if } \frac{1}{2} < K < \sqrt{2}, \end{cases} \tag{3.29}$$

and  $\Delta\phi(K)$  is defined in (3.7). Using the identity for the difference of the sines of two angles and assuming that

$$\frac{nC(\alpha, \beta, K)}{2\sqrt{2}\Gamma \sin \frac{n\Delta\phi(K)}{2}} < 1, \tag{3.30}$$

the transverse zeros of  $\Delta^n \hat{\mathcal{H}}_D(v; \mu_0)$  can be written as

$$\begin{aligned} \phi_{n,1}^l &= -\frac{n\Delta\phi}{2} - \cos^{-1} \frac{nC(\alpha, \beta, K)}{2\sqrt{2}\Gamma \sin \frac{n\Delta\phi(K)}{2}} + (2l+1)\pi, \quad l \in \mathbb{Z}, \\ \phi_{n,2}^m &= -\frac{n\Delta\phi}{2} + \cos^{-1} \frac{nC(\alpha, \beta, K)}{2\sqrt{2}\Gamma \sin \frac{n\Delta\phi(K)}{2}} + (2m+1)\pi, \quad m \in \mathbb{Z}. \end{aligned} \tag{3.31}$$

To obtain the zero sets defined in (2.32), we will consider the particular members of the above families of zeros which fall in the interval  $[\phi_s, \phi_s + 2\pi]$ :

$$\begin{aligned} \phi_{-,1}^n &= \phi_s + 2\pi - [\phi_s + 2\pi - \phi_{-,1}^0] \bmod 2\pi, \\ \phi_{-,2}^n &= \phi_s + 2\pi - [\phi_s + 2\pi - \phi_{-,2}^0] \bmod 2\pi, \end{aligned} \tag{3.32}$$

with  $\phi_s$  defined in (3.26). Introducing the angles

$$\phi_{+,1}^n = [\phi_{-,1}^n + n\Delta\phi] \bmod 2\pi, \quad \phi_{+,2}^n = [\phi_{-,2}^n + n\Delta\phi] \bmod 2\pi, \tag{3.33}$$

we obtain the zero sets in (2.32) in the form

$$\begin{aligned} \hat{Z}_-^n &= \hat{Z}_-^n = \{(\eta, \phi) \mid \phi \in \{\phi_{-,1}^n, \phi_{-,2}^n\}\}, \quad n \geq 1, \\ \hat{Z}_+^n &= \hat{Z}_+^n = \{(\eta, \phi) \mid \phi \in \{\phi_{+,1}^n, \phi_{+,2}^n\}\}, \quad n \geq 1. \end{aligned} \tag{3.34}$$

Our particular choice for the interval  $[\phi_s, \phi_s + 2\pi]$  in the above construction is related to the upcoming construction of a layer sequence within  $\hat{S}_\zeta$  which will be similar to that of Section 3.1.2. This time, however, the zero sets  $\hat{Z}_\pm^n$  do not necessarily intersect  $\hat{S}_\zeta$ , and we must have a way to decide whether this intersection occurs or not. If we pick the zeros of the energy difference function  $\Delta^n \hat{\mathcal{H}}_D$  from the interval  $[\phi_s, \phi_s + 2\pi]$ , then we can check the above intersection based on the following observation: in the set  $[-\eta_0, \eta_0] \times [\phi_s, \phi_s + 2\pi]$  all points which lie within  $\hat{S}_\zeta$  have  $\hat{\mathcal{H}}_D$  energies lower than  $\hat{\mathcal{H}}_D(0, \phi_s)$ . Hence, to construct an energy sequence similar to (3.15), one can select  $\hat{h}_0 = \hat{\mathcal{H}}_D(0, \phi_s)$  and define  $\hat{h}_n$  as in (3.15), then proceed the same way as in Section 3.1.2. The reason why this whole construction is dependent on the right choice of zeros is that  $\hat{\mathcal{H}}_D$  is originally defined on the real line and it does not define a single valued “energy” on the annulus  $\hat{A}$ .

Finally, there is one more observation we want to make for later purposes. Note that if a point  $\hat{b}_-$  is contained in  $\hat{Z}_-^n \cap \hat{S}_\zeta$ , then the point  $\hat{b}_+ \in \hat{Z}_+^n$  with the same  $\eta$  coordinate will be contained in  $\hat{S}_\zeta$ . This follows from the fact that, by construction,  $\hat{b}_+$  has the same or lower  $\hat{\mathcal{H}}_D$ -energy than  $\hat{b}_-$ , so if  $\hat{b}_-$  lies in the domain  $\hat{S}_\zeta$ , so does  $\hat{b}_+$ . As a result, it follows from Theorem 2.2 that for small  $\varepsilon > 0$  any multi-pulse orbit “taking off” from the open domain  $\Pi_\varepsilon(\hat{S}_\zeta)$  of the slow manifold  $\mathcal{A}_\varepsilon^R$  will ultimately land on the same domain.

### 3.2.3. Pulse numbers

We first note that from (3.30) we directly obtain an upper bound on the pulse numbers:

$$n < \frac{\sqrt{2}}{|\zeta|\Delta\phi}, \tag{3.35}$$

which shows that for arbitrarily small dissipation and for  $K \in (0, 1/2) \cup (1/2, \sqrt{2})$  the infinite homoclinic tree we found in Section 3.1.2 will break into a finite tree. As in Section 3.1.2, the pulse number of any internal orbit outside  $\hat{S}_\zeta$  is equal to 1. Furthermore, as we discussed in the previous subsection, for the orbits inside  $\hat{S}_\zeta$  one can adapt the same construction as in Section 3.1.2 to classify them based on their pulse numbers. Namely, one can again define the energy sequence

$$\hat{h}_0 = \hat{\mathcal{H}}_D(0, \phi_s; \mu_0), \quad \hat{h}_n = \min(\hat{\mathcal{H}}_D(0, \phi_{-,1}^n; \mu_0), \hat{\mathcal{H}}_D(0, \phi_{-,2}^n; \mu_0)). \tag{3.36}$$

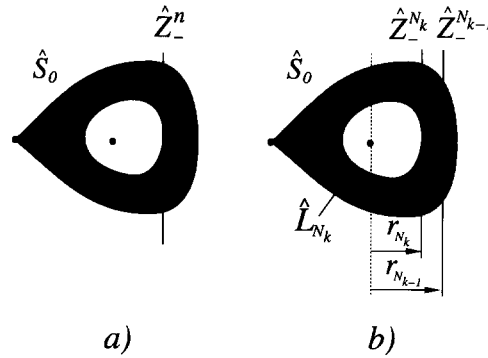


Fig. 17. The construction of the layer sequence for (3.23)<sub>ε=0</sub>.

Then the definitions of  $\{\hat{A}_n\}$ , the pulse sequence  $\{N_k\}$  and the layer sequence  $\{\hat{L}_{N_k}\}$  are the same as in the undamped case (see Figs. 17a,b). This time, however, all these sequences are finite by (3.35). As earlier, we obtain that for any periodic orbit  $\hat{\gamma} \subset \hat{L}_{N_k}$  the pulse number is  $N(\hat{\gamma}) = N_k$ .

To simplify our discussion, we now restrict our analysis to the case of  $\alpha = \beta > 0$ . As we indicated earlier, this is the case of mode independent damping which is relevant if we want to relate our results to the numerical experiments of Bishop et al. As seen from (3.28), we have

$$C(\alpha, \alpha, K) = -8\alpha K^2 \Delta\psi(K) > 0, \tag{3.37}$$

which shows that the zeros defined in (3.31) can be rewritten as

$$\begin{aligned} \phi_{n,1}^l &= -\frac{n\Delta\phi}{2} - \cos^{-1} \frac{-2\sqrt{2}\zeta n K^2 \Delta\psi(K)}{\sin \frac{n\Delta\phi(K)}{2}} + (2l+1)\pi, \quad l \in \mathbb{Z}, \\ \phi_{n,2}^m &= -\frac{n\Delta\phi}{2} + \cos^{-1} \frac{-2\sqrt{2}\zeta n K^2 \Delta\psi(K)}{\sin \frac{n\Delta\phi(K)}{2}} + (2m+1)\pi, \quad m \in \mathbb{Z}. \end{aligned} \tag{3.38}$$

This form of the zero sets enables us to construct the pulse numbers and layer radii, for fixed values of the dissipation factor  $\zeta$ , as a function of the parameter  $K$ . The results are shown in Figs. 18a,b for various values of  $\zeta$ . In these plots we used  $K$  as bifurcation parameter, as opposed to the phase shift  $\Delta\phi$  in Section 3.1.2. For comparison with the undamped case, in Fig. 18a we also show the pulse number and layer radius diagrams for zero damping ( $\zeta = 0$ ) as a function of  $K$ . In all plots in Figs. 18a,b the layer radii are defined as

$$r_{N_k} = \min(|\phi_c - \phi_{-1}^{N_k}|, |\phi_c - \phi_{-2}^{N_k}|). \tag{3.39}$$

In these diagrams one can see a gradual break-up of the homoclinic tree as the dissipation is increased compared to the forcing. The meaning of the pulse diagram is again the same: it shows the existing multi-pulse solutions which approach the slow manifold  $\mathcal{A}_\varepsilon^R$  positively and negatively as the wave number  $K$  changes. According to Theorem 2.2, the layer radius diagram shows the approximate distances of the “take-off” points of these multi-pulse orbits from the slow sink on  $\mathcal{A}_\varepsilon^R$  (see also the phase portrait in Fig. 17b).

### 3.2.4. Jump sequences

The argument we gave in Section 3.1.2 cannot be used here to give a general description of jump sequences in the dissipative case. Instead of attempting to classify all the possible jump sequences, we only note that for small values of  $\alpha = \beta$  the multi-pulse orbits are continuations of those constructed in Section 3.1, hence the corresponding jump sequences are all alternating.

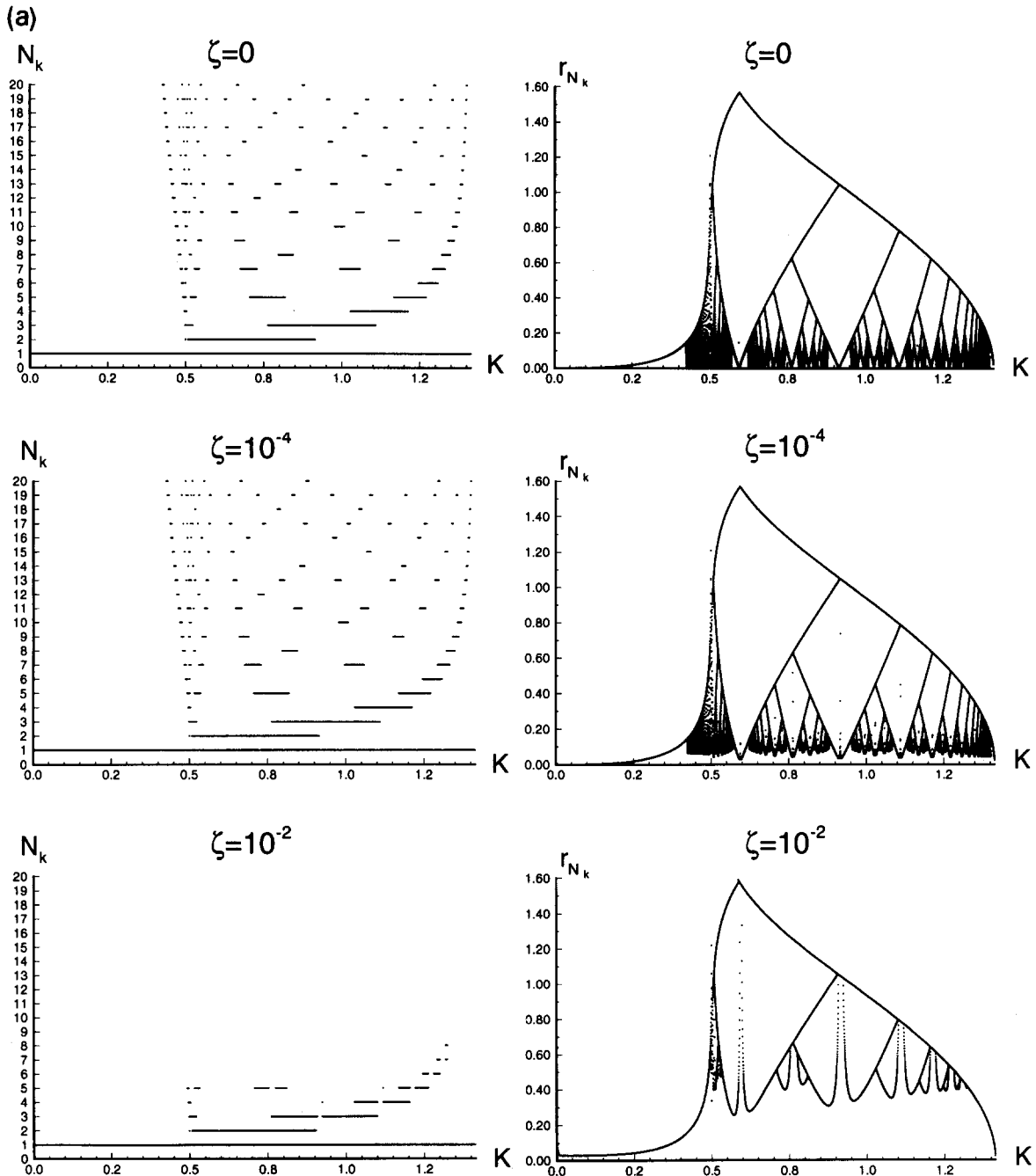


Fig. 18. The pulse sequence and the layer radius sequence as functions of the wave number  $K$  for the damped-forced two-mode model.

### 3.2.5. Multi-pulse orbits

Having the construction of the pulse sequence  $\{N_k\}$  at hand, we know about the existence and bifurcations of multi-pulse orbits which positively and negatively approach the slow manifold  $\mathcal{A}_\varepsilon^R$ . We have constructed the zero sets  $\hat{\mathcal{Z}}^N$  in a way such that any  $\hat{\mathcal{Z}}^{N_k}$  will necessarily have a nonempty intersection with the homoclinic

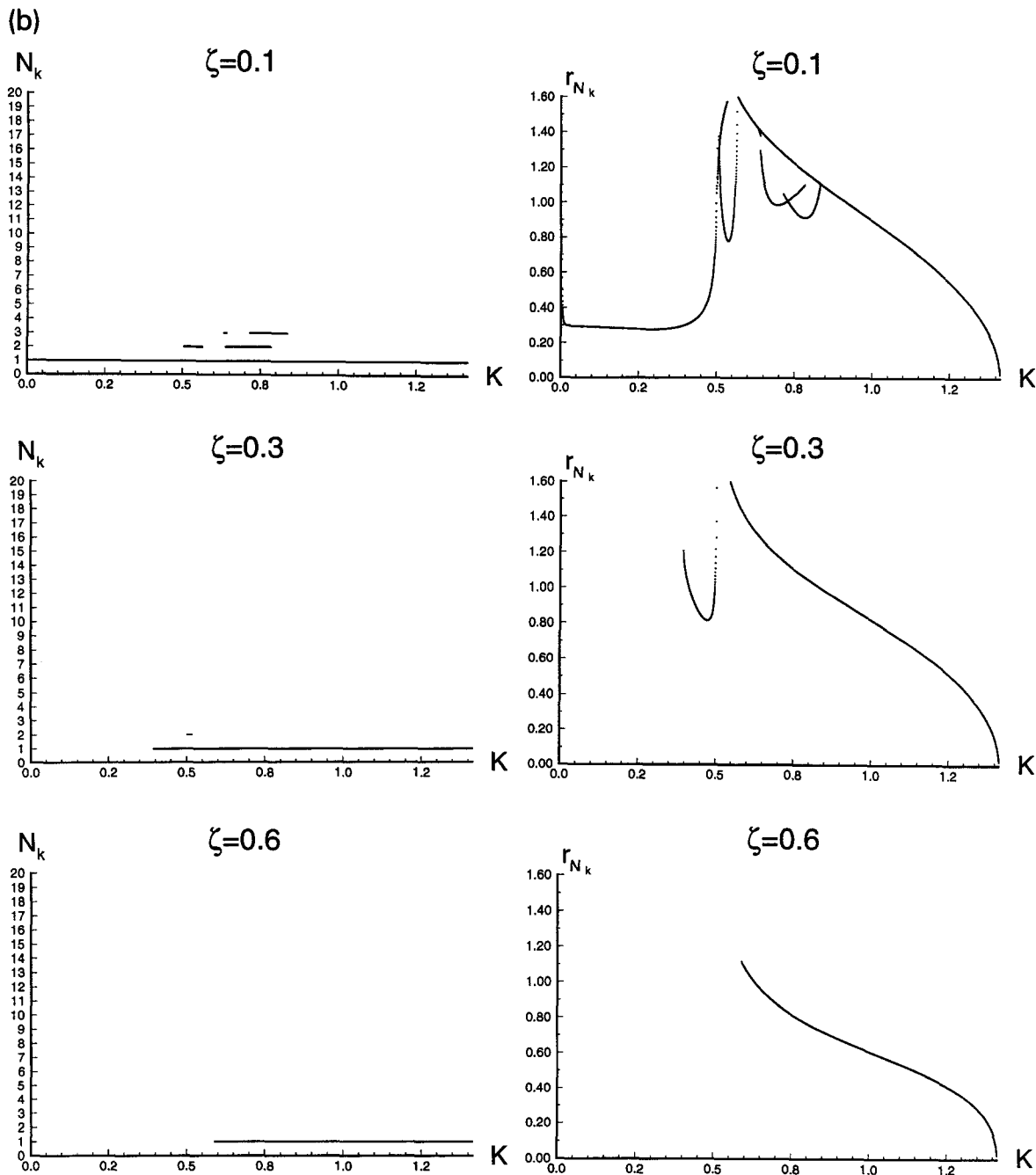


Fig. 18 — continued.

domain  $\hat{S}_\zeta$  of the reduced system  $(3.23)_{\varepsilon=0}$ . It follows from Theorem 2.2 that for any slow orbit  $\gamma_\varepsilon^- \subset \mathcal{A}_\varepsilon^R$  intersecting  $\Pi_\varepsilon^{-1}(\hat{Z}^{N_k} \cap \hat{S}_\zeta)$  there exist two  $N_k$ -pulse orbits,  $y_\varepsilon^{N_k+}$  and  $y_\varepsilon^{N_k-}$  which negatively approach  $\gamma_\varepsilon^-$ . As we discussed in Section 3.2.1, the projection of the dissipative slow dynamics on  $\mathcal{A}_\varepsilon^R$  onto the annulus  $\hat{A}$  can be approximated by the dissipative reduced system (3.23) with its phase portrait shown in Fig. 17b. Regarding this phase portrait we observe the following: for any  $N_k > 0$  one can select  $\varepsilon > 0$  sufficiently small, so that a

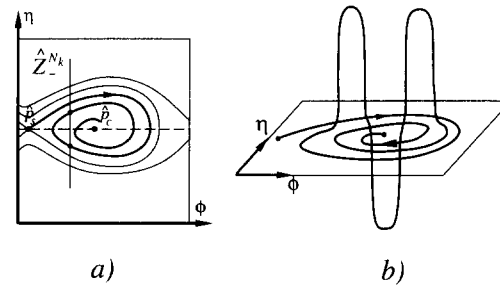


Fig. 19. The construction of a structurally stable, multi-pulse heteroclinic orbit for  $N_k = 3$ .

component of the unstable manifold  $W^u(p_s)$  (which perturbs from the homoclinic loop of  $(3.23)_{\varepsilon=0}$ ) intersects the zero set  $\hat{Z}_-^{N_k}$  transversally in at least two points, which lie inside  $\hat{S}_0$  in some  $\mathcal{O}(1)$  distance from  $\partial\hat{S}_0$ . Furthermore, the angle of the intersection is of  $\mathcal{O}(1)$  as  $\varepsilon \rightarrow 0$  and the number of intersections tends to infinity as  $\varepsilon \rightarrow 0$  (see Fig. 19a). As a result, there will be  $N_k$ -pulse orbits in the forced-damped two-mode model which negatively approach the unstable manifold of a saddle-type equilibrium on  $\mathcal{A}_\varepsilon^R$  (this equilibrium is a saddle-saddle when viewed in the full four dimensional phase space). Consequently, these multi-pulse orbits are negatively asymptotic to a saddle-saddle lying in the resonance band.

The next question is the forward asymptotics of these multi-pulse orbits, which can be easily answered based on our final observation in Section 3.2.2. In this way one can conclude that any of the multi-pulse orbits backward asymptotic to the saddle-saddle will be forward asymptotic to a “slow” sink on  $\mathcal{A}_\varepsilon^R$  whose existence can be inferred from the phase portrait of the dissipative reduced system shown in Fig. 17b. The geometry of such a multi-pulse orbit is shown in Fig. 19b. Note that the construction of these orbits is robust with respect to small changes in the parameters; hence the multi-pulse orbits are *structurally stable*. Another way of seeing this is that they lie in the generically one dimensional intersection of the two dimensional unstable manifold of the saddle-saddle with the three dimensional stable manifold of the saddle-sink. Using Theorem 2.2, we obtain the following main result for the damped-forced two-mode model.

**Theorem 3.2.** For some fixed value of the parameters  $K$  and  $\Gamma$  and  $\alpha = \beta$  let us consider the pulse sequence defined in Section 3.2.3 and plotted as a function of  $K$  in Figs. 18a,b for some values of  $\zeta = \alpha/\Gamma$ . Then for any element  $N_k$  of this sequence there exists  $\varepsilon_0$  such that for  $0 < \varepsilon < \varepsilon_0$  the following hold:

- (i) The damped-forced system (1.6) has at least four structurally stable,  $N_k$ -pulse jumping orbits homoclinic to the slow manifold  $\mathcal{A}_\varepsilon^R$ . These orbits are backward asymptotic to a saddle-saddle-type equilibrium and are forward asymptotic to a saddle-sink-type equilibrium (see Fig. 19b). The actual number of such orbits tends to infinity as  $\varepsilon \rightarrow 0$ .
- (ii) The distance of the take-off points of the above multi-pulse orbits from the saddle-sink is  $\mathcal{O}(\varepsilon^{\frac{1}{2}})$ -close to  $r_{N_k}$ , where  $r_{N_k}$  is defined in (3.39), and plotted in Figs. 18a,b.

The direct visualization of multi-pulse orbits guaranteed by the above theorem is much harder than in the Hamiltonian case, because we cannot use energy conservation any more. Firstly, this makes it more difficult to keep track of the accuracy of the simulation. Secondly, three coordinates are no longer enough to demonstrate the intersection of the stable and unstable manifold of orbits on  $\hat{\mathcal{A}}_\varepsilon$ . Thirdly, once the multi-pulse orbits get very close to the slow manifold before their first pulse in backward time and after their last pulse in forward time, they slow down and will be driven away from  $\mathcal{A}_\varepsilon^R$  near its unstable manifold. To counteract this tendency, one has to use a more sophisticated numerical algorithm combined with careful error estimates, which can be a subject of a separate paper. Even without this, however, one can use the simulation pictures Figs. 13–15 to get

an idea of the nature of jumping orbits in the dissipative case, since they stay close to Hamiltonian multi-pulse orbits during their finite times of flight outside a neighborhood of the slow manifold. As far as the behavior these orbits is considered in a thin “boundary layer” near  $\mathcal{A}_\varepsilon^R$ , one can refer to Fig. 19b to see their forward and backward asymptotics.

#### 4. Conclusions

In this paper we proved the existence of multi-pulse orbits in a two-mode truncation of the damped-forced nonlinear Schrödinger equation. These orbits are backward and forward asymptotic to  $\mathcal{A}_\varepsilon^R$ , a two dimensional “slow” manifold of solutions. In the case of no damping,  $\mathcal{A}_\varepsilon^R$  can be chosen invariant, and it carries a slow pendulum-type dynamics. As we have seen in Section 3.1, the open domain of “rotational” periodic orbits of this pendulum dynamics can be divided into layers indexed by integer numbers  $N_k$ , for which we derived a recursive formula depending on the system parameters (see Figs. 9a–c for a plot of the results). The layer structure has the following property: for any slow periodic orbit  $\gamma_\varepsilon$  lying in the  $N_j$ th layer there exist at least four transverse, jumping  $N_k$ -pulse homoclinic orbits doubly asymptotic to  $\gamma_\varepsilon$ . All these orbits have alternating jump sequences (see Definition 2.1), but these sequences start with +1 for two of them and with –1 for the rest. By the transversality of these homoclinic orbits, we established the existence of Smale horseshoes and hence chaotic dynamics on Cantor sets on most energy levels intersecting the slow manifold  $\mathcal{A}_\varepsilon^R$ . For our methods to work we have to exclude energy levels which intersect  $\mathcal{A}_\varepsilon^R$  in small amplitude periodic solutions lying in a  $\mathcal{O}(\sqrt{\varepsilon})$  neighborhood of the center of the slow pendulum dynamics. The nature of the dynamics on such energy levels is still an open question, although its influence on the numerically observable jumping is not significant. To describe how the layer structure changes as the phase shift  $\Delta\phi$  varies, we presented a recursive construction to calculate the inner angular radii of all existing layers (see Fig. 10). As the magnitude of the pulses considered tends to infinity, this bifurcation diagram approaches an infinite binary tree shown in Fig. 11. We illustrated the results by numerical simulation visualizing the intersection of stable and unstable manifolds of periodic orbits.

We also studied the multi-pulse behavior in the damped-forced two-mode model. Although our general results are valid for all values of  $\alpha$  and  $\beta$ , we chose to discuss them in more detail for the case when  $\alpha = \beta$ . In terms of the underlying PDE, this condition means that all modes are equally damped, as was assumed in the numerical study of Bishop et al. [2]. We have shown that if the dissipation factor  $\zeta = \alpha/\Gamma$  is not too large, then there exist structurally stable multi-pulse jumping orbits in the damped-forced two-mode model, which connect a saddle-saddle-type equilibrium to a saddle-focus-type equilibrium. These orbits admit three different time scales: 1. fast alternating bursts in the form of pulses near the two unperturbed homoclinic manifolds; 2. intermediate slow-downs between two subsequent pulses; 3. very slow asymptotic approach to the saddle-saddle in backward time and to the saddle-focus in forward time. The distribution of existing pulses is shown in Figs. 18a,b together with the bifurcation of take-off distances from the saddle-focus as the wave number  $K$  varies. These plots show how the homoclinic tree found for the Hamiltonian limit of pure forcing breaks up as the damping coefficients increase compared to the forcing amplitude.

We believe that our results give a more direct explanation for the jumping behavior observed in the two-mode model than related earlier studies, which were all concerned with the existence of single-pulse homoclinic orbits, and found such orbits only on codimension one sets of the parameter space. In contrast to all these results described in Section 1, the orbits found in this paper are *structurally stable*. Furthermore, as it is shown in Haller and Wiggins [15], the multi-pulse orbits constructed by the energy-phase method spend an  $\mathcal{O}(\log(1/\sqrt{\varepsilon}))$  time in a neighborhood of the slow manifold between subsequent pulses. Using standard Gronwall estimates one can

therefore conclude the existence of an open set of initial conditions of measure  $\mathcal{O}(\sqrt{\varepsilon})$  near any multi-pulse orbit described above, such that trajectories starting from that open set exhibit the same jumping behavior for finite times as the underlying multi-pulse orbit. Hence the presence of multi-pulse orbits we constructed provide a *numerically observable* jumping mechanism. This distinguishes our construction from that of Kaper and Kovačič [23] who constructed multi-pulse orbits near resonance bands using a modified Melnikov-type method and the Exchange Lemma of Jones, Kaper, and Kopell [22]. Their multi-pulse orbits lie in an exponentially small neighborhood of single-pulse orbits and spend times of  $\mathcal{O}(1/\sqrt{\varepsilon})$  within a small neighborhood of the slow manifold between all their subsequent pulses.

Finally, it is of great importance to find a similar multi-pulse jumping behavior for the damped-forced nonlinear Schrödinger equation itself. Based on the work of Li [25], one expects this to be possible, since the geometric structure of the full PDE has many elements in common with that of the two-mode truncation studied in this paper. Hence the next major step in tackling the dynamics of the damped-forced NLS is to generalize the energy-phase method to infinite dimensions. This work is in progress and will appear in Haller [17].

## Acknowledgment

We would like to thank Dave McLaughlin for many insightful remarks and helpful discussions. We also thank the Academic Computing Facility of New York University for access to its facilities. G.H. is grateful to Ed Friedman and Estarose Wolfson at ACF, NYU for their valuable help and advice.

## References

- [1] M.J. Ablowitz and B.M. Herbst, On homoclinic structures and numerically induced chaos for the nonlinear Schrödinger equation, *SIAM J. Appl. Math.* 50 (1990) 339–351.
- [2] A.R. Bishop, M.G. Forest, D.W. McLaughlin and E.A. Overman, A modal representation of chaotic attractors for the driven, damped pendulum chain, *Phys. Lett. A* 144 (1990) 17–25.
- [3] A.R. Bishop, R. Flesch, M.G. Forest, D.W. McLaughlin and E.A. Overman, Correlations between chaos in a perturbed sine-Gordon equation and a truncated model system, *SIAM J. Math. Anal.* 21 (1990) 1511–1536.
- [4] A. Cascon, J. Koiller and S.M. Rezende, Bifurcations of mode equations: spin waves, *Physica D* 54 (1991) 98–124.
- [5] P. Constantin, C. Foias and R. Temam, *Integral Manifolds and Inertial Manifolds for Dissipative Partial Differential Equations* (Springer, New York, 1988).
- [6] N.M. Ercolani, M.G. Forest and D.W. McLaughlin, Geometry of the modulational instability, Part III: Homoclinic Orbits for the periodic sine-Gordon equation, *Physica D* 43 (1990) 349–384.
- [7] N.M. Ercolani and D.W. McLaughlin, Towards a topological classification of integrable PDE's, in: *The Geometry of Hamiltonian Systems* (Springer, New York, 1991).
- [8] Z.C. Feng and P.R. Sethna, Symmetry breaking bifurcations in resonant surface waves, *J. Fluid Mech.* 199 (1989) 495–518.
- [9] Z.C. Feng and P.R. Sethna, Global bifurcation and chaos in parametrically forced systems with one-one resonance, *Dynam. Stab. Syst.* 5 (1990) 201–225.
- [10] Z.C. Feng and P.R. Sethna, Global bifurcations in the motion of parametrically excited thin plates, *Nonlinear Dynam.* 4 (1993) 398–408.
- [11] Z.C. Feng and S. Wiggins, On the existence of chaos in a class of two-degree-of-freedom, damped, strongly parametrically forced mechanical systems with broken  $O(2)$  symmetry, *ZAMP* 44 (1993) 201–248.
- [12] N. Fenichel, Persistence and smoothness of invariant manifolds for flows, *Ind. Univ. Math. J.* 21 (1971) 193–225.
- [13] G. Haller and S. Wiggins, Orbits homoclinic to resonances: the Hamiltonian case, *Physica D* 66 (1993) 298–346.
- [14] G. Haller and S. Wiggins, Whiskered tori and chaos in resonant Hamiltonian normal forms, in: *Normal Forms and Homoclinic Chaos*, Fields Institute Publications (1995), to appear.
- [15] G. Haller and S. Wiggins,  $N$ -pulse homoclinic orbits in perturbations of resonant Hamiltonian systems, *Arch. Rat. Mech. Anal.* (1995), to appear.
- [16] G. Haller and S. Wiggins, Geometry and chaos near resonant equilibria of 3DOF Hamiltonian systems, *Physica D*, submitted. (1994).
- [17] G. Haller, Irregular jumping and heteroclinic orbits in the perturbed nonlinear Schrödinger equation, in preparation.

- [18] P. Holmes, A nonlinear oscillator with a strange attractor, *Phil. Trans. R. Soc. A* 292 (1979) 419–448.
- [19] P. Holmes and J. Marsden, A partial differential equation with infinitely many periodic orbits: chaotic oscillations of a forced beam, *Arch. Rat. Mech. Anal.* 76 (1981) 135–166.
- [20] P. Holmes and J. Marsden, Horseshoes in perturbations of Hamiltonian systems with two degrees of freedom, *Commun. Math. Phys.* 82 (1982) 523–544.
- [21] P. Holmes, Chaotic motion in a weakly nonlinear model for surface waves, *J. Fluid. Mech.* 162 (1986) 365–388.
- [22] C.K.R.T. Jones, J. Kaper and N. Kopell, Tracking invariant manifolds up to exponentially small errors, preprint (1993).
- [23] T.J. Kaper and G. Kovačič, Multiple-pulse homoclinic orbits near resonance bands, preprint (1993).
- [24] G. Kovačič and S. Wiggins, Orbits homoclinic to resonances, with an application to chaos in the damped and forced sine-Gordon equation, *Physica D* 57 (1992) 185–225.
- [25] Y. Li, Chaotic Dynamics in Partial Differential Equations, Ph.D. Thesis, Princeton University (1993).
- [26] Y. Li and D.W. McLaughlin, Morse and Melnikov functions for NLS PDE's, *Commun. Math. Phys.* 162 (1994) 175–214.
- [27] J. Marsden and M. McCracken, *The Hopf Bifurcation and Its Applications* (Springer, New York, 1976).
- [28] D. McLaughlin, E.A. Overman II, S. Wiggins and C. Xiong, Homoclinic orbits in a four dimensional model of a perturbed NLS equation: a geometric singular perturbation study, *Dynamics Reported* (1993), submitted.
- [29] A. Mielke, *Hamiltonian and Lagrangian Flows on Center Manifolds*, Lecture Notes in Mathematics, Vol.1489 (Springer, New York, 1991).
- [30] A.H. Nayfeh and P.F. Pai, Non-linear, non-planar parametric responses of an inextensional beam, *Int. J. Non-lin. Mech.* 24 (1989) 139–158.
- [31] C. Robinson, Horseshoes for autonomous Hamiltonian systems using the Melnikov integral, *Ergod. Th. Dynam. Sys.* 8, pp. 395–409.
- [32] W.-M. Tien and N.S. Namamchivaya, Nonlinear dynamics of a shallow arch under periodic excitation II: 1:1 internal resonance, *Int. J. Non-Lin. Mech.* 29(3) (1994) 367–386.
- [33] S. Wiggins, *Global Bifurcations and Chaos-Analytical Methods* (Springer, New York, 1988).
- [34] S. Wiggins, *Normally Hyperbolic Invariant Manifolds in Dynamical Systems* (Springer, New York, 1994).
- [35] X.L. Yang and P.R. Sethna, Non-linear phenomena in forced vibrations of a nearly square plate: antisymmetric case, *J. Sound Vib.* 155 (1992) 413–441.
- [36] V.E. Zakharov and A.B. Shabat, Exact theory of two dimensional self-focusing and one dimensional self-modulation of waves in nonlinear media, *Sov. Phys. JETP* 34 (1972) 62–69.